

## TOPICAL REVIEW

# Adhesive elastic contacts: JKR and more

**E Barthel**

Surface du Verre et Interfaces, CNRS/Saint-Gobain, UMR 125, 93330, Aubervilliers Cedex, France

E-mail: [etienne.barthel@saint-gobain.com](mailto:etienne.barthel@saint-gobain.com)

Received 19 February 2008, in final form 19 May 2008

Published 31 July 2008

Online at [stacks.iop.org/JPhysD/41/163001](http://stacks.iop.org/JPhysD/41/163001)**Abstract**

Since the early 1990s, adhesive contact mechanics has emerged as an area of considerable interest in nano- and bio-sciences. Here we review the methods which have been developed in the past 75 years to account for adhesive interactions in elastic contact problems. Emphasis is given to the connection between the local, physical mechanism of adhesion and the macroscopic, mechanical loading. The discussion centres on the contact equations. In an attempt to provide a broad view of the field, we outline the key concepts and their progressive developments, starting from the approximate calculation by Derjaguin in 1934 and ending with recent results for coated systems and time dependent materials, through the well established DMT and JKR models.

**Introduction**

Adhesive contacts play a central role in many technological areas. Efficient manufacturing processes require a tight control over the contamination of surfaces by particles: wafer cleaning, for example, is a key technology in semiconductor technology [1]. Energy efficient mechanical devices [2] and reliable micromechanical systems [3] demand better control over friction and lubrication. Key phenomena such as particle immobilization or release in filtration [4], controlled positioning in reproduction devices [5], settling of bio-organisms on surfaces in health [6] or bio-technologies must be better understood for further progress.

Such an ambitious programme offers at least two facets. The first issue is the physical and chemical properties of the surfaces—how do two surfaces interact?—and their engineering by surface modification. The second issue is the impact of surface interactions on the global mechanical response of the particle: for a given loading, will the particle be captured, can it be released? Here, one of the core problems is the adhesive contact. The rising impact of the JKR model (Johnson *et al* [7], figure 1), starting in the 1990s, reveals the steeply growing relevance of small scale adhesive contact theories in physics and biology.

**Method.** In the adhesive contact problem, the issue is to account for the attractive coupling between surfaces in the mechanical description of the contact. In this paper, we review

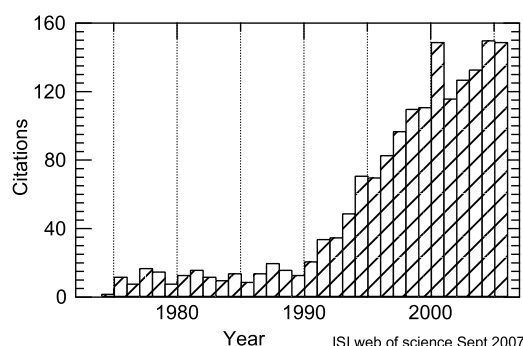


**Figure 1.** Number of citations to the JKR model.

some of the methods which have been developed over the last 75 years. Except in section 3.2.3, the discussion is limited to linear elastic systems and their immediate extensions. For clarity it is focused on a restricted set of models. They are all somehow evolved from the Hertz model for adhesionless contact [8] and revert to it in the proper limit. We think these models are simpler and more likely to be of practical use. They are also easier to generalize to more complex mechanical responses. In fact, our selection of models is also directed by the underlying derivation method. They are readily amenable to the Hankel transform method pioneered by Sneddon [9–11]. However, we did not try to provide a rigorous derivation of each result but the interested reader will find hints in a small technical appendix.

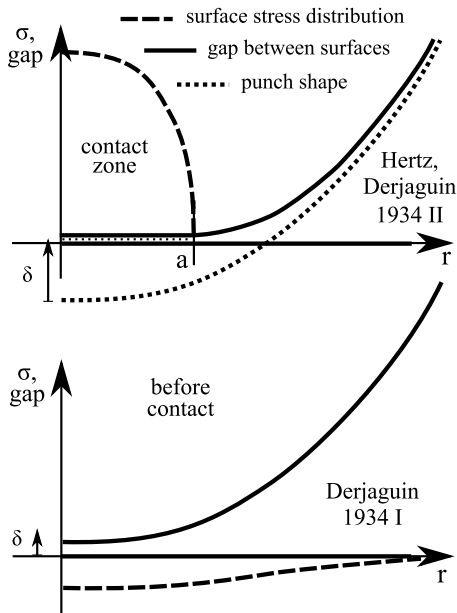


**Figure 2.** (Top) The geometry of the Hertzian contact. (Bottom) Interaction between curved surfaces before contact (Derjaguin approximation).

In a typical elastic contact, the three macroscopic contact variables (load  $F$ , penetration  $\delta$  and contact radius  $a$ , figure 2) obey two relations called the *contact equations*. For a given model, these relations delineate its specific behaviour. We will not detail the features of each model, for which ample literature is available. The single distinctive feature we will mention is the pull-out force. In contrast, we focus on the form adopted by the contact equations. In this way we can both stress the key ideas common to all models and show how they differ in relation to the underlying physical assumptions. Finally, the relevance of the theoretical developments is evidenced by specific experimental results which have been selected for illustration purposes.

*Outline.* Section 1 is mostly a brief account of the standard models but we first discuss an early method by Derjaguin [12] which is simple but suitable for order of magnitude calculations only. The bulk of the section is devoted to the DMT (Derjaguin–Muller–Toporov) model [13] and the JKR (Johnson–Kendall–Roberts) model [7]. Typical experimental applications of the JKR model are also detailed.

The applicability of the DMT or JKR models is restricted to specific types of interactions between surfaces. Expanding on these interactions to account for *arbitrary* adhesive coupling, section 2 provides an overview of more recent developments. The experimental motivations are described. The general contact equations are formulated and a very simple but efficient solution is suggested. More generally, we provide an account of the more technical self-consistent calculation of the ensuing surface deformations, insisting on the common threads and trends encountered in the various versions. The practical implications for data analysis are discussed.

Section 3 develops this approach beyond homogeneous, time independent materials. Complex systems feature

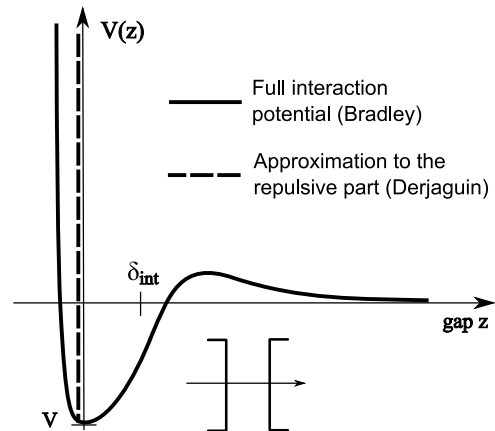


**Figure 3.** Typical interaction potential between flat surfaces (Bradley, full self-consistent model) and approximation (dashed) to the repulsive part (Derjaguin, restricted self-consistent model).

mechanical responses which depend upon either lengthscale (thin film) or timescale (viscoelastic). We show how the adhesive stresses couple to a local mechanical response which—in the general case—differs from the macroscopic response. We discuss implications for adhesive contacts: the impact is minor for non-homogeneous materials but in many cases it is very significant for time dependent materials.

## 1. Level 1—basic results

### 1.1. Interactions—contact

The first adhesive contact models appeared in the 1930s. The topic emerged out of steady progress in surface physics and chemistry and a sharper perception of the nature of the interactions between surfaces (for a short account see [14]). Bradley [15] and Derjaguin [12] almost simultaneously proposed models for the adhesion of spheres. Interestingly the main contrast between the Derjaguin and Bradley approaches is still echoed in present day research. Let us denote  $V(z)$  the interaction potential between flat surfaces of unit area separated by a distance  $z$  (figure 3). Bradley considered the full interaction potential  $V(z)$  between two surfaces, including attractive and repulsive contributions to the potential. Summation of the interaction stresses over the curved bodies, assumed rigid, provide the interaction force [15]. When surface deformation is taken into account, the Bradley method evolves in the so-called full self-consistent method [16]. Derjaguin also considered the attractive part of the potential but treated the repulsive part differently [12]. He assumed that this repulsive contribution is so steep that the surfaces cannot interpenetrate. As a result [17] the boundary conditions specify the surface normal displacement—instead of the surface normal stress—inside the contact zone, exactly as in the Hertz model for the adhesionless elastic contact [8]. The Derjaguin approach is the prototype of the so-called restricted self-consistent method [16]. This approximation is the background of this paper. We only occasionally refer to fully self-consistent results or to finite element calculations.

*1.1.1. Contact problems.* Starting with the adhesionless contact model, we consider an axisymmetric punch pressed against a rigid flat surface (figure 2). In the restricted self-consistent method:

- (i) the contact problem involves *mixed boundary conditions*: the normal surface stresses are prescribed *outside* the contact zone while the normal surface displacements are prescribed *inside* (figure 2(top)).
- (ii) the contact radius  $a$  is not prescribed directly but depends upon the loading: it grows with increasing load  $F$  and increasing penetration  $\delta$ . The contact problem is *geometrically non-linear*.

A solution is an equilibrium stress field (and its associated displacement field) which matches the boundary conditions. It provides the set of two relations between the three macroscopic contact variables (contact equations). Before we discuss the impact of adhesion, we first identify expressions for the contact equations in the absence of adhesion.

*Adhesionless contact equations—Hertz.* For a sphere of radius  $R$ , the punch shape  $f(r)$  is approximately

$$f(r) = \frac{r^2}{2R}. \quad (1)$$

Hertz [8] demonstrated that an ellipsoidal distribution of contact stresses, inside the contact zone, flattens this elastic sphere. The relation between penetration and contact radius<sup>1</sup> is

$$\delta_H(a) = \frac{a^2}{R} \quad (2)$$

and the relation between the force and the contact radius is

$$F_H(a) = \frac{4E^*a^3}{3R}, \quad (3)$$

$E^*$  is the reduced modulus  $E/(1 - \nu^2)$  where  $E$  is Young's modulus and  $\nu$  the Poisson ratio. Equations (2) and (3) are the contact equations for the adhesionless (and frictionless) contact of an elastic sphere on a rigid plane. A more detailed account of the Hertz result and its generalization to other punch shapes can be found in [appendix A.2.1](#).

The *gap*, denoted  $h_H(r)$  in the adhesionless contact theory, is the distance between opposite surfaces outside the contact zone. The gap shape results from the deformation of the punch shape  $f(r)$  (equation (1)) by the non-local elastic response to the contact stresses (see [appendix A.2.1](#)) and adhesive interaction stresses if present. Indeed, the gap will be of considerable significance when the interactions between surfaces are included in the contact theory.

## 1.2. Adhesive contact of an elastic sphere

The question is now: how can we include adhesion in such a contact problem?

<sup>1</sup> It is sometimes argued that equation (2) is geometric in nature because it does not involve mechanical parameters. Notwithstanding, it is a mechanical relation as shown when non-homogeneous materials are considered (section 3.1.1).

*1.2.1. Derjaguin 1934—Adhesion.* The first model was proposed in the lesser-known second part of the otherwise famous 1934 paper [12] by Derjaguin. There he assumes that the contact stresses and the gap shape are given by the Hertz predictions. Adhesion is very simply included as the *adhesion energy*  $w$  expended in separating a unit area of contacting surfaces (figure 2(top)). Denoting  $\mathcal{E}_H$  the elastic energy for the Hertz contact, the total energy of the system is now

$$\mathcal{E}(\delta) = \mathcal{E}_H(\delta) - w(\pi a^2) \quad (4)$$

and the force is calculated as

$$F = \frac{d\mathcal{E}}{d\delta}. \quad (5)$$

By assumption, the Hertz relation (equation (2)) between contact radius and penetration is preserved. Thus the Hertzian force is simply offset by a constant  $-\pi w R$ . The contact equations (equations (2) and (3)) become

$$\delta_D = \delta_H(a), \quad (6)$$

$$F_D = F_H(a) - \pi R w. \quad (7)$$

*Pull-out force.* The *pull-out force* is defined as the force required to separate the surfaces. As tensile forces are counted negative, it is the minimum of the force-penetration curve. It is a useful characteristics of the various adhesive models. For the Derjaguin 1934 model,

$$F_{\text{pullout}} = -\pi R w \quad (8)$$

and pull out occurs at  $a = 0$ .

*Relevance.* The Derjaguin 1934 model for the adhesive contact (equations (6)–(8)) is not exact but, as noted by Johnson and coworkers [7], it is useful for order of magnitude estimates of elastic adhesive contact properties.

*Orders of magnitude.* Equation (8) demonstrates that adhesion effects are not negligible for externally applied loads of the order of  $\pi w R$  or less [18]. If this adhesion force is compared with the gravity force, adhesion will become significant for smaller particle radii, namely,

$$R < \sqrt{\frac{w}{\rho g}}, \quad (9)$$

where  $\rho$  is the density and  $g$  the acceleration of gravity. For typical values ( $w = 0.1 \text{ J m}^{-2}$ ,  $\rho = 1 \times 10^3 \text{ kg m}^{-3}$ ) this cross-over radius, which is similar to a capillary length, will be of the order of millimetres. Surface energy terms must be considered at smaller scales<sup>2</sup>; larger particles remain negligibly affected by adhesive contributions.

In this regime, the typical contact radius can be calculated assuming zero externally applied load ( $F_D = 0$ ). Then compressive and tensile stresses balance each other and (equations (3) and (7))

$$a \simeq \left( \frac{\pi w R^2}{E^*} \right)^{1/3} \quad (10)$$

<sup>2</sup> In many cases roughness issues can notably alter this conclusion.

and the magnitude of the contact stresses is

$$\sigma_c \simeq \left( \frac{w E^*{}^2}{\pi^2 R} \right)^{1/3}. \quad (11)$$

For a soft material ( $E^* = 10$  MPa), this means a contact radius of the order of  $30 \mu\text{m}$  and contact stresses  $\sigma_c \simeq 0.5$  MPa. A full normalization scheme has been developed by Maugis [19] (appendix A.3) while interesting alternative schemes have been proposed by Triadis [20].

**1.2.2. Derjaguin approximation.** The pull-out force predicted by Derjaguin (equation (8)) is at variance with another expression derived in the very same paper. In the first part of [12], Derjaguin calculated the force acting between a sphere and a plane at small separation but *before* actual contact (figure 2(bottom)). Although it does not involve actual mechanical contact, this model is of interest here for the manner the attractive interactions between surfaces are introduced.

The surfaces are at close proximity, but not touching. They are separated by a distance  $\delta > 0$  and attract each other by a radial distribution of surface stresses  $\sigma_z(r)$ . The total force is simply

$$F_{\text{ext}} = 2\pi \int_0^{+\infty} dr r \sigma_z(r). \quad (12)$$

**Interaction potential.** Following Derjaguin [12] we assume that the adhesive stresses derive from an interaction potential  $V(z)$ , as in section 1.1 (figure 2(b)). The characteristic features of this interaction potential are its amplitude, typically

$$V_0 = -V(0) \quad (13)$$

and its decay length  $\delta_{\text{int}}$ . The interaction stresses acting between these flat surfaces is

$$\sigma(z) = -\frac{dV}{dz}(z). \quad (14)$$

We denote  $\sigma_0$  the amplitude of the attractive interaction stresses. Then

$$\sigma_0 \simeq \frac{V_0}{\delta_{\text{int}}}. \quad (15)$$

**The Derjaguin approximation.** Assuming that the surfaces are *rigid*, and neglecting the impact of the curvature of the surface on the interaction, the radial stress distribution is

$$\sigma_z(r) = \sigma(h(r)) = -\frac{dV}{dz}(h(r)), \quad (16)$$

where  $h(r)$  denotes the gap. Since here we have no surface deformation but a simple rigid body displacement  $\delta$ , the gap is  $h(r) = f(r) + \delta$ . Then, for the sphere (equation (1)), equation (12) becomes

$$F_{\text{ext}}(\delta) = 2\pi R V(\delta). \quad (17)$$

This is the famous Derjaguin approximation [12] which has found widespread use in surface forces measurements [21].

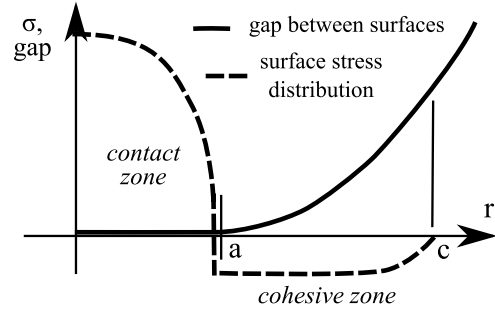


**Figure 4.** The geometry of the DMT adhesive contact. The attractive interactions act over the cohesive zone, an annulus (radius  $c$ ) surrounding the contact zone (radius  $a$ ). The DMT model applies if  $c \gg a$ .

It states that the force between the sphere and the plane is proportional to the interaction potential between flat surfaces at the same distance. The proportionality coefficient is the sphere radius.

Taking the separation between surfaces  $\delta = 0$ , we obtain an evaluation of the pull-out force

$$F_{\text{pullout}} = -2\pi R V_0. \quad (18)$$

Now, from the definitions of  $w$  (section 1.2.1) and  $V$ , assuming  $V(+\infty) = 0$ , it is clear that  $w = V_0$ . As a result the pull-out forces resulting from equations (8) and (18) differ by a factor of 2 as already noted in [12]. As a first step towards understanding this discrepancy we now investigate how the attractive force exerted on the sphere by the plane is affected when the surfaces are actually pressed against each other and develop a contact zone.

**1.2.3. Another model—DMT.** In 1983, Derjaguin and coworkers proposed another adhesive contact theory called DMT [22, 23], which is the ‘natural’<sup>3</sup> extension of the Derjaguin approximation (section 1.2.2) when contact stresses are included. As with the Derjaguin 1934 model [12], the authors assume that the Hertzian stress distribution and deformation fields apply but that the adhesive interaction stresses (figure 4) result in an additional force, which is now computed in the manner of the Derjaguin approximation. Then the set of contact equations (equations (2) and (3)) becomes

$$\delta_{\text{DMT}} = \delta_H(a), \quad (19)$$

$$F_{\text{DMT}} = F_H(a) + F_{\text{ext}}(a), \quad (20)$$

where the outer force term

$$F_{\text{ext}}(a) = 2\pi \int_a^{+\infty} dr r \sigma_z(r) \quad (21)$$

is the direct extension of equation (12). This additional force term can be evaluated as follows. Assuming that the adhesive interaction stresses derive from the interaction potential  $V(z)$  as in the Derjaguin approximation (section 1.2.2, figure 3), the spatial distribution of attractive stresses is expressed as

$$\sigma_z(r) = -\frac{dV}{dz}(h_H(r)), \quad (22)$$

<sup>3</sup> Starting in 1974 [13], the development of the DMT theory is a muddled issue. For a detailed account see [24].



where  $h_H(r)$  is the gap of the Hertz contact (section 1.1.1). For a given potential  $V(z)$  the adhesive force  $F_{\text{ext}}(a)$  can be calculated numerically [23]. However, as we show below, this step usually turns out unnecessary.

The pull-out force for the DMT theory is

$$F_{\text{pullout}} = -2\pi R w \quad (23)$$

because at  $a = 0$ , by assumption, the DMT theory merges with the Derjaguin approximation (section 1.2.2).

**Validity.** In the DMT theory, the compressive contact stresses, inside the contact zone, result in the surface deformation necessary to match the contact boundary conditions. In contrast it is assumed that the attractive stresses, outside the contact zone, do not bring about deformation. This consideration places a restriction on the interaction stresses:  $\sigma_0$  must be small compared with the contact stresses and we infer that the DMT theory is valid for  $\sigma_0 \ll \sigma_c$  (equation (11)) which leads to the condition (equation (15))

$$\delta_{\text{int}} \gg \left( \frac{\pi^2 w^2 R}{E^*} \right)^{1/3}. \quad (24)$$

The DMT model will typically be relevant for small, rigid spheres and long range interactions. For example, for a glass microsphere ( $R = 100 \mu\text{m}$ ,  $E^* = 1 \times 10^{11} \text{ GPa}$ ) the cross-over decay length above which DMT applies is a reasonable  $\delta_{\text{int}} = 1 \text{ nm}$ .

Note that the right-hand side of inequality (24) is actually the penetration for zero applied load (use equations (6) and (10)). Denoting by  $c$  the outer radius of the region over which the attractive interaction stresses act (the so-called cohesive zone—figure 4) we can compare  $c$  and the contact radius  $a$ . Indeed  $\delta_{\text{int}} \simeq c^2/2R$  while  $\delta = a^2/R$ . Then a condition of validity for the DMT model equivalent to equation (24) is that the contact zone is much smaller than the cohesive zone [25]:

$$c \gg a. \quad (25)$$

**The sphere—DMT in the Maugis manner.** As a result the contact zone has little impact on equation (21) and a simple and accurate version of the DMT theory proposed by Maugis [19] is to take  $F_{\text{ext}}$  constant:

$$F_{\text{ext}}(a) = -2\pi R w. \quad (26)$$

**Puzzling facts about the DMT theory.** Similar considerations developed for other punch shapes must now be mentioned. Assuming punch shapes of the form

$$f(r) = \frac{r^n}{K_n} \quad (27)$$

the pull-out force for low stress values (small  $\sigma_0$ ) obeys a power law behaviour  $\sigma_0^m$  with  $m = (n - 2)/n$  [20, 26]. For instance, if  $n = 1$  (cone)  $F_{\text{pullout}} \rightarrow +\infty$  and if  $n > 2$  (cubic)  $F_{\text{pullout}} \rightarrow 0$  [27]. As a result, in this weak interaction regime, *except* for the paraboloid (sphere), the pull-out force is remarkably sensitive to the interaction range.

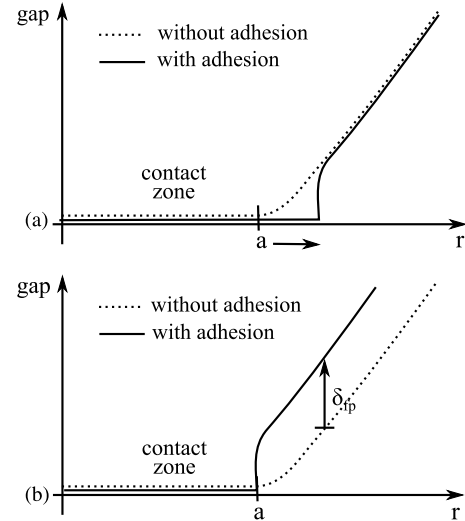


**Figure 5.** Schematic illustration of the neck formed at the contact edge. In a thought experiment, an adhesionless contact has been formed. When adhesion is switched on the contact area spreads out (a). The contact radius is preserved if a (negative) flat punch displacement restrains contact growth (b).

**Status of the adhesion energy in the DMT model.** As these more general results demonstrate, the DMT model relies on the interplay between interaction potential and punch shape. The pull-out force is *not* controlled by contact area creation or destruction as assumed in the Derjaguin 1934 model. The adhesion energy  $w$  as a thermodynamic variable coupled to contact area is *not* the relevant concept: in the DMT model the pull-out force derives from the motion of the punch in the long range *interaction potential*. Strictly speaking, the parameter relevant for adhesion is the amplitude of the interaction potential  $V_0$  rather than the adhesion energy  $w$ . In the DMT theory the punch displacement directly couples to the interaction potential.

**1.2.4. Surface energy transfer—JKR.** Performing experiments on rubber friction in the Cavendish laboratory in Cambridge, Roberts distinctly observed the formation of a neck around the contact area of adhesive hemispheres [7].

The phenomenon can be understood in analogy to wetting. Imagine a thought experiment performed with a soft rubber-like sphere. Let us start from an adhesionless contact (section 1.1.1) and turn the adhesive interactions on. At *constant penetration*  $\delta$  the contact area increases (figure 5(a)). Alternatively, to keep the *contact area* constant, one needs to pull the sphere back some distance (figure 5(b)). This pull-back motion at fixed contact radius is a flat punch displacement  $\delta_{\text{fp}}$  which accounts for the neck experimentally observed. Indeed the flat punch solution is singular at the contact edge (appendix A.2.2): the surface displacement exhibits a square root singularity outside the contact zone, the surface stress an inverse square root singularity inside.

If the neck height  $\delta_{\text{fp}}$  is large enough, which is typically the case for soft materials, then it spans the full interaction range, of order  $\delta_{\text{int}}$  (figure 3). Then a contact radius variation  $da$  results in a transfer of work  $w d(\pi a^2)$  from the contact

zone, in complete analogy to a peel test for example. The neck singularity is precisely the energy transfer mechanism which is lacking in the original Derjaguin 1934 method (section 1.2.1). The energy transfer is controlled by the neck height  $\delta_{fp}$ : energy minimization [7, 28] shows that the neck height  $\delta_{fp}$  must obey

$$2\pi aw = E^* \delta_{fp}^2. \quad (28)$$

This equation, which is proved in section 3.1.2, is the core of the original JKR model [7]. As a result of the local treatment of the adhesive process, the neck height depends upon the elastic response and adhesion energy but not upon the punch shape. In the JKR model the relevant thermodynamic variable is the *contact area*, coupled to the adhesion energy.

In summary, in the JKR model, the flat punch term contributes a peeling action at the contact edge. The adhesive parameter involved is indeed the adhesion energy  $w$ , the energy required to create surfaces.

*Validity of the JKR model.* Combining equations (10) and (28) we observe that the JKR flat punch displacement is

$$\delta_{fp} \simeq \left( \frac{\pi w^2 R}{E^*} \right)^{1/3}. \quad (29)$$

Tabor [29] suggested introducing a parameter comparing this flat punch displacement to the decay length of the interaction potential  $\delta_{int}$  (equation (15)). Denoting this parameter  $\lambda$ , we have

$$\lambda \equiv \frac{\delta_{fp}}{\delta_{int}} \simeq \frac{\sigma_0}{\left( \frac{w E^*}{\pi R} \right)^{1/3}}. \quad (30)$$

This parameter is identical to the stress ratio introduced earlier (section 1.2.3). It measures the impact of the interaction stresses on the surface deformations<sup>4</sup>. The JKR case is obtained for large  $\lambda$  while small  $\lambda$  values characterize the DMT regime (section 1.2.3). In contrast to DMT, the JKR theory applies when interaction stresses are large and the materials compliant.

*Contact equations.* Linear superposition of the adhesionless contact and the flat punch solutions (appendix A.2.2) provides the contact equations

$$\delta(a) = \delta_H(a) + \delta_{fp}, \quad (31)$$

$$F(a) = F_H(a) + F_{fp}(a). \quad (32)$$

In contrast to the previous models the flat punch term offsets both Hertzian force *and* penetration. The correction to the Hertzian force, the flat punch force term, is given by

$$F_{fp}(a) = \delta_{fp} S(a). \quad (33)$$

It is linear in  $\delta_{fp}$  because for a flat punch the contact radius  $a$  is constant: the flat punch contact problem is geometrically linear. The flat punch (or contact) stiffness (appendix A.2.2) is

$$S(a) = 2aE^*. \quad (34)$$

<sup>4</sup> Tabor called this parameter  $\mu$ . For a detailed listing of the equivalent definitions of the Tabor parameter see [30].

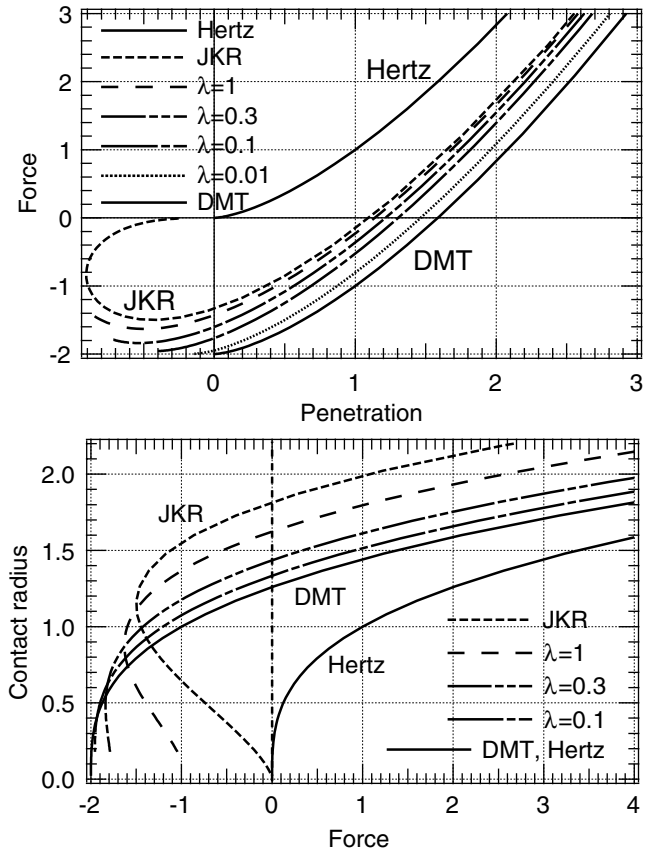


**Figure 6.** Contact relations for Hertz, DMT and JKR models. Also shown are double-Hertz models with different values of the Tabor parameter  $\lambda$ .

The form adopted in the set of equations (31) and (32) is quite general and can be used for different punch shapes [26, 31, 32], although the sphere is the shape of choice for most experiments.

*The case of the paraboloid—pull-out force.* For the specific case of the contact of a homogeneous elastic sphere (approximated by a paraboloid as in section 1.2.2) the contact equations result from equations (2), (3), (28), (31) and (32):

$$\delta_{JKR}(a) = \frac{a^2}{R} - \sqrt{\frac{2\pi aw}{E^*}}, \quad (35)$$

$$F(a)_{JKR} = \frac{4E^* a^3}{3R} - 2\sqrt{2\pi E^* w a^3}, \quad (36)$$

which is the original JKR result [7]. The pull-out force can be calculated by minimization of the total force (equation (36)), which results in

$$F_{pullout} = -\frac{3}{2}\pi w R. \quad (37)$$

Note, however, that in contrast to previous models, pull out occurs at a finite contact radius with a characteristic size given approximately by equation (10).

The contact relations in the JKR and the DMT models are plotted in figure 6 along with other cases which are described later. Normalization has been carried out according to appendix A.3: in particular, the force is normalized to  $\pi w R$ . Observe how the DMT model is obtained by a translation of

the Hertz force curves by  $-2$  along the force axis while the JKR flat punch term induces shifts both along the force *and* the displacement axis.

### 1.3. The JKR model—some applications

**1.3.1. The JKR test.** The various adhesive contact theories are often identified by the relation they provide between pull-out force and adhesion energy. In practice, however, the direct use of relations such as equations (21) or (37) to infer adhesion energies, although widely spread, is suspect. Indeed rupture occurs at a point of *instability*. The consequences are twofold. Fluctuations will significantly affect the results [33] while the dynamics of the interfacial response will impact the pull-out force in a non-trivial manner [34].

It is much more powerful to actually record data in the *stable* adhesive contact region (i.e. before contact rupture) and analyse them with a given contact model. Building upon the so-called JKR test, various experimental devices have been developed where the contact radius can be monitored as a function of the applied load to infer the adhesive properties of various types of surfaces [35–37]. The main application of such devices is to characterize surface modification through adhesion.

**1.3.2. The dynamics of adhesive contact rupture.** As an example of JKR experiment we reproduce a typical curve for contact radius versus load by Deruelle and coworkers [38] for PDMS lenses on a rigid substrate (figure 7). This curve should be compared with figure 6(b). Clearly the loading and unloading paths do not superimpose. In addition the system was unloaded stepwise: after a displacement step the system is held at constant displacement for some time during which the contact radius decreases gradually.

These results evidence irreversibility and also kinetic effects: after each step the contact radius decreases and then slows down to a nearly equilibrium value. It has been shown [36, 38–40] that the experiments can be rationalized if the notion of a velocity dependent adhesion is substituted to the thermodynamic notion of (reversible) adhesion energy  $w$ . The macroscopic deformation of the PDMS lens very accurately conforms to JKR theory so that one can use JKR theory to extract an effective adhesion energy which depends only upon the contact radius velocity  $\dot{a} = da/dt$  but not upon the contact radius  $a$ . The equilibrium JKR theory as described in section 1.2.4 is perfectly adequate here because the behaviour of the bulk of the system is elastic and the time dependent and irreversible phenomena are lumped into the contact edge response (more on this in section 3.3.2).

**1.3.3. Energy release rate.** Since the simple adhesion energy picture must be abandoned we take a broader point of view and consider the problem under the mechanical angle. We calculate the elastic energy released per unit area when the contact edge recedes. This quantity, called the *energy release rate* and denoted  $G$  is the driving force for contact edge propagation [36]. If equilibrium holds, then  $G = w$ . More generally the energy release rate can be used to quantify the

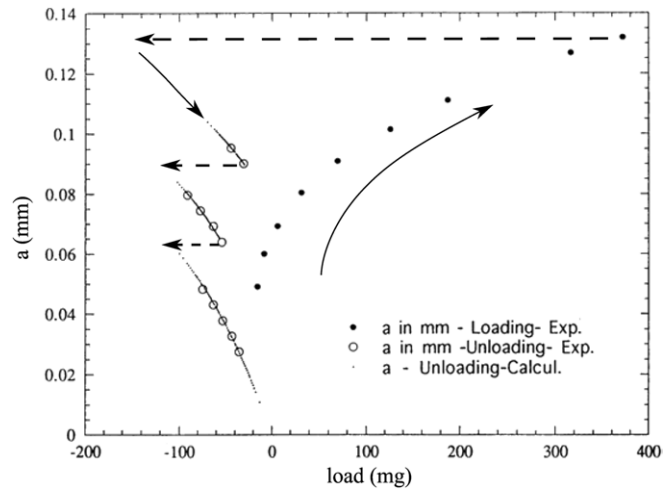


**Figure 7.** JKR experiment: note the large hysteresis between contact formation and rupture. Pull out was carried out step by step (dashed arrows) whereby it is shown how the effective adhesion measured depends upon the contact edge velocity. (Adapted from [38] with permission from the American Chemical Society.)

effective adhesion in non-equilibrium contact phenomena: the dynamics of  $G$  and its dependence upon waiting time reveal the relevant interfacial processes.

A more powerful method to calculate  $G$  is introduced in section 3.1.2. Here  $G$  is simply inferred from the contact equations (35) and (36), substituting  $G$  to  $w$ . Combining equations (28) and (32) results in

$$G(\dot{a}) = \frac{E^*}{2\pi a} \left( \frac{F(a) - F_H(a)}{S(a)} \right)^2. \quad (38)$$

In practice  $a$ ,  $\dot{a}$  and  $F(a)$  are measured directly;  $F_H(a)$  and  $S(a)$  can be calculated from  $a$  through equations (3) and (34) to assess  $G(\dot{a})$ .

A relation similar to equation (38) can be constructed from the penetration equation (31). The full series of homologous relations can be found in [32] for other punch geometries as well. Note, however, that in practice the force-based energy release rate (equation (38)) is the more robust (section 3.2.3).

## 2. Level 2—the contact edge—a closer view

### 2.1. JKR and DMT do not fit all

Atomic force microscopy (AFM) is often used to probe surface interactions at the local scale. Indeed AFM measurements provide good examples of the growing effect of surfaces as the size of the system decreases [41]. Extensive reviews have considered many aspects of AFM force measurements (see for instance [42] for force measurements and [43] for friction). Consider an AFM tip with a radius of curvature ca 10 nm: it is clear that the range of the interactions is no longer very small compared with the system size. Simultaneously the stiffness of the material (silica or silicon nitride) is much larger than for PDMS spheres. As a result the conditions of application of the JKR model, which requires significant local deformation of the surfaces under the action of the interaction stresses (equations (24) or (30)), may not be fulfilled. AFM

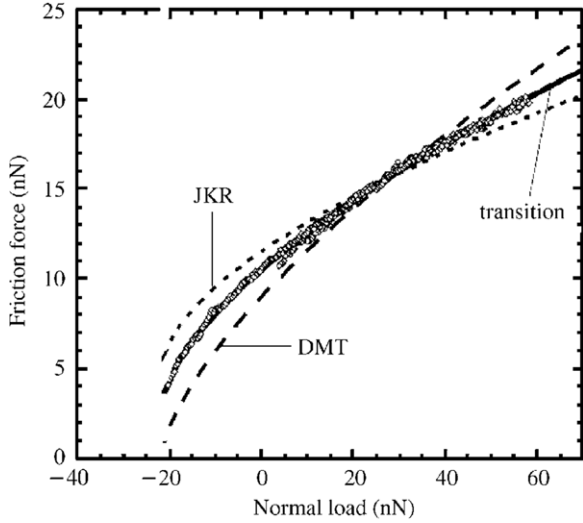


**Figure 8.** AFM friction force measurements as a function of normal load. The JKR and DMT best fits are shown. In these experimental conditions it seems necessary to take into account the finite range of the interactions. (After [33] with permission from Brill.)

experiments are a good playground to find a non-JKR adhesive contact.

More generally, AFM force measurements call for extensive modelling. Indeed, AFMs are easy to operate, but provide only limited information in contact experiments. Because of the very low stiffness of the cantilever, the deflexion at contact contains only information on the *force* and does not allow for an accurate measurement of the *penetration*. Of course the *contact radius* cannot be measured directly either and one is usually left with a single contact variable, the force, a shortcoming which precludes more elaborate fitting procedures such as exemplified in section 1.3.2: with AFM the bare use of pull-out forces, with all the drawbacks mentioned above (section 1.3.1), is widespread.

This situation has been circumvented in certain cases by the measurement of the *lateral stiffness* [44–46] which is proportional to the contact radius. Measuring the *friction force* is also a way to assess contact area. A typical example is shown in figure 8 where attempts have been made to fit a contact curve by a DMT or a JKR model [33]. Although the system explored in this specific example is complex, such results stress the need for more involved modelling of the adhesive contact.

## 2.2. Adhesive contact models for interactions of intermediate range

**Macroscopic equations.** Here we assume that the interactions have intermediate range, comparable to the flat punch displacement. Alternatively, the magnitude of the attractive interaction stresses is comparable to the contact stresses. Then the interaction stresses contribute to surface deformations but without reaching fully into the JKR regime. In this case the contact equations are a plain superposition of JKR and DMT terms [47]:

$$\delta(a) = \delta_H(a) + \delta_{fp}, \quad (39)$$

$$F(a) = F_H(a) + F_{fp}(a) + F_{ext}(a). \quad (40)$$

$F_{ext}$  obeys equation (21) as for DMT and  $F_{fp}$  equation (33) as for JKR. However, because we are not in a full JKR regime, the flat punch displacement is *not* determined by equation (28). Similarly, because we are not in a full DMT regime,  $F_{ext}$  is *not* given by equation (26). A standard solution is presented in section 2.3 but we first mention another interesting—and simpler—option.

**A mixed model.** Following Schwarz [48], we assume the attractive interaction results from the superposition of a very short range interaction in the JKR manner (adhesion energy  $w_1$ ) and a very long range interaction in the DMT manner (adhesion energy  $w_2$ ). The total adhesion energy is  $w = w_1 + w_2$ . From the results in section 1, linear superposition allows us to conclude that in equations (39) and (40)

$$2\pi a w_1 = E^* \delta_{fp}^2 \quad (41)$$

and

$$F_{ext}(a) = 2\pi R w_2. \quad (42)$$

With equation (33) these two equations completely specify the solution. The resulting behaviour for varying ratios of the adhesive contributions  $w_1/w_2$  has been studied in detail by Schwarz [48] who has shown that it compares favourably with the results of more classical interaction models.

## 2.3. Inside the cohesive zone—accounting for the interactions

We now deal with more orthodox attractive interactions which inevitably entail more elaborate calculations. Indeed, once the functional form of the attractive interaction has been given, it is usually difficult to compute the details of the cohesive zone. Two methods are briefly described. The generic features of the solutions are highlighted in a specific example. The impact of finite range interactions is then reviewed and their practical relevance discussed.

**2.3.1. Exact self-consistency equation.** An equation similar to equations (16) or (22) may be used:

$$\sigma_z(r) = \sigma(h(r)) = -\frac{dV}{dz}(h(r)). \quad (43)$$

Here, because the elastic response is non-local, the gap  $h(r)$  results from the compressive contact stresses *and* the tensile adhesive interaction stresses (equation (A.18)). Since the latter in turn depends upon the gap (equation (43)), the result is a strongly non-linear equation. Strictly speaking



a self-consistent calculation of the full deformation and stress fields inside the cohesive zone is called for [17].

**2.3.2. Approximate self-consistency equation.** A more interesting form for the self-consistency equation emerges from the definition of the surface stresses (equation (14)). Then

$$w = \int_a^{+\infty} dr \sigma_z(r) \frac{\partial}{\partial r} h(r). \quad (44)$$

Equation (44) provides opportunities for useful approximate models because it does not explicitly involve the full functional form of the interaction potential (as in equation (43)) but only the adhesion energy [17]. We assume a given *spatial distribution* for  $\sigma_z(r)$ ; more complex distributions may occur but typically its amplitude is  $\sigma_0$  and it extends over the cohesive zone (i.e. between  $a$  and  $c$ , figure 9(b)). For adequate choices of the functional form of  $\sigma_z(r)$ , the analytical integration of equation (44) can be carried out. Typically  $\sigma_0$  is a parameter,  $a$  the running contact variable, and the self-consistent calculation needs only determine the cohesive zone radius  $c$  so that force and penetration may be calculated. Thus, for each value of  $a$ , a single scalar  $c$  has to be determined instead of the full stress distribution field inside the cohesive zone. This *weak formulation* of the self-consistency equation leads to incomparably lighter numerical calculations than exact self-consistency (section 2.3.1).

**2.3.3. Double Hertz.** As an example of self-consistency equation in the weak formulation, we briefly comment on the so-called ‘double-Hertz’ model as proposed by Greenwood [49]. In this model the spatial distribution of attractive stresses obeys an ellipsoidal distribution

$$\sigma(r) = \begin{cases} -\sigma_0 \sqrt{\frac{c^2 - r^2}{c^2 - a^2}} & \text{if } a \leq r \leq c, \\ 0 & \text{if } c < r. \end{cases} \quad (45)$$

Then

$$\delta_{fp} = -\sigma_0 \frac{\pi}{2E^*} \sqrt{c^2 - a^2} \quad (46)$$

and

$$F_{ext}(a) = \frac{\pi \sigma_0}{\sqrt{c^2 - a^2}} \left( -\frac{2}{3} c^3 - \frac{1}{3} a^3 + c^2 a \right). \quad (47)$$

For a given magnitude of the interaction stresses  $\sigma_0$ , the cohesive zone radius  $c$  can be determined as a function of the contact radius  $a$  with the self-consistency equation (equation (44)) which in this case reads [49]

$$w = \frac{1}{3} \left( \frac{1}{R} + \frac{\pi \sigma_0}{2E^* \sqrt{c^2 - a^2}} \right) \frac{\sigma_0}{\sqrt{c^2 - a^2}} I_H(c, a), \quad (48)$$

where  $I_H(c, a) = (c - a)^2(c + 2a)$ .

**General considerations.** The structure of this particular self-consistency equation (48) is generic. The right-hand member of equation (48) consists of two terms. The first term is linear in the interaction stresses and depends only upon the shape of the punch (radius  $R$ ). It originates from the work of the adhesive interaction stresses in the surface displacement induced by the contact stresses ( $W_{contact}$ ). The second term is quadratic in the interaction stresses and originates from the work of the interaction stresses in the displacements they themselves induce ( $W_{self}$ ). This ‘self-energy’ of the interaction stresses does not depend upon the shape of the punch. The governing parameter is the ratio of these two terms  $R\sigma_0/E^*\sqrt{c^2 - a^2}$  which determines the relative weight of  $W_{contact}$  and  $W_{self}$ . Using equation (10), we can consistently identify this normalized interaction stress with the Tabor parameter  $\lambda$  (section 1.2.4).

**Limit cases.** The first term has DMT character while the second term is reminiscent of JKR. Indeed from equations (39) and (40) and (46)–(48) we can derive the DMT and JKR limits. When  $\sigma_0 \rightarrow 0$ ,  $W_{contact}$  is dominant,  $c$  is large compared with  $a$ ,  $\sigma_0 c^2 \rightarrow 3Rw$ ,  $\delta_{fp} \rightarrow 0$  and  $F_{ext} \rightarrow -2\pi R w$ . The gap is unaltered by the interaction stresses and the solution to the self-consistency equation (44) is the Hertzian gap: this is the DMT limit.

When  $\sigma_0 \rightarrow \infty$ ,  $W_{self}$  is dominant,  $c - a$  is small compared with  $a$ ,  $\sigma_0^2(c - a) \rightarrow 4E^*w/\pi$ ,  $\delta_{fp} \rightarrow -\sqrt{2\pi a w/E^*}$  and  $F_{ext} \rightarrow 0$ . This is the JKR limit. Beyond this specific example, the limit can actually be demonstrated quite generally [17, 20]: for large  $\lambda$  and if there is *one single decay length*  $\delta_{int}$ , equation (28) is recovered.

**Gap—surface stress.** Examples of gap and surface stress distributions for various values of  $\lambda$  are displayed in figure 9. Note how the finite size of the interaction zone regularizes the typical JKR flat punch singularity at the edge of the contact. The finite interaction range plays a similar role in wetting problems [50]. For an identical normalized contact radius, the penetration turns from positive to negative as the interaction becomes more and more JKR like (large  $\lambda$ ). The corresponding force curves are plotted in figure 6. As  $\lambda$  goes from zero to infinity, a continuous transition between DMT and JKR is followed. In particular, the pull-out force evolves continuously from  $2\pi w R$  to  $3/2\pi w R$ . This transition can be followed in more details by plotting the flat punch displacement  $\delta_{fp}$  and the outer force contribution at pull out as a function of the normalized attractive interaction stress (i.e. the Tabor parameter  $\lambda$ ) (figure 10).  $\delta_{fp}$  saturates at the JKR limit  $-(2/3)^{1/3}$  which is about  $-1.747$  for large  $\lambda$  and slowly goes to zero as  $\lambda$  decreases. The outer force is zero for large  $\lambda$ , decreases with decreasing  $\lambda$  and practically reaches  $-2$  when  $\lambda < 0.02$ .

**2.3.4. The DMT–JKR transition** The continuous transition between DMT and JKR configurations suggested by Tabor [29] has been first explicitly demonstrated by Muller [51]. Subsequently, more refined calculations have confirmed the transition [19, 20, 24, 49, 52, 53]. A complete map of

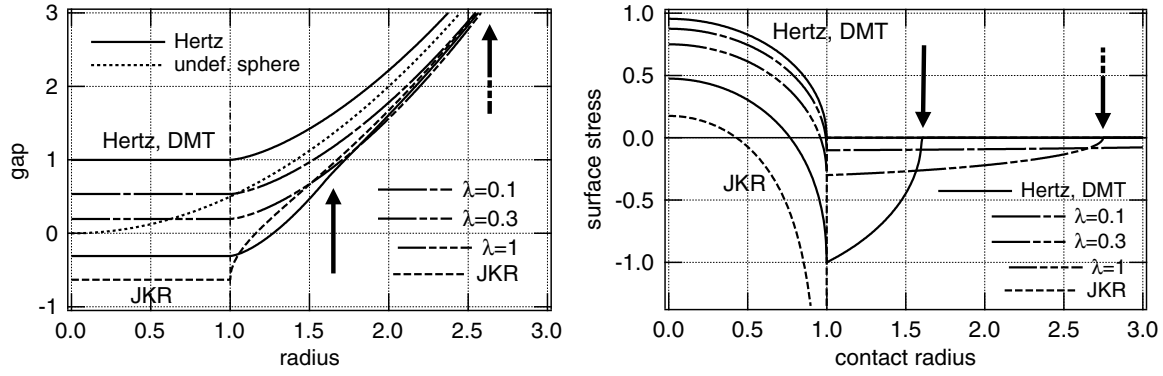


**Figure 9.** Normalized gap (left) and stress distribution (right) as a function of Tabor parameter  $\lambda$  for a normalized contact radius  $a = 1$  (double-Hertz model). The arrows point to the cohesive zone radius for  $\lambda = 1$  and  $0.3$ . The gaps all converge to the undeformed sphere (dashed) at large radii. The penetration required to maintain contact radius turns from positive to negative as  $\lambda$  increases from  $0$ . Note also how the finite interaction range regularizes the JKR singularity.

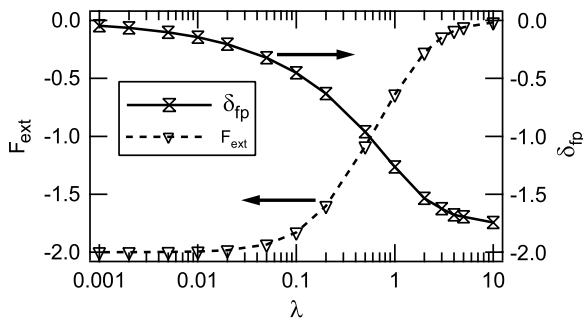


**Figure 10.** Adhesive contributions to the contact equations (equations (39) and (40)) with finite interaction range: outer force term (left axis) and flat punch displacement at pull out as a function of the Tabor parameter  $\lambda$  (double-Hertz model).

the domains of validity of the various models has been proposed [18]. The wealth of theoretical evidence for the transition is paralleled by a paucity of experimental demonstrations. The reason is the difficulty in tuning the characteristic interaction stress at fixed adhesion energy. The most convincing results have been obtained through SFA experiments which demonstrated the impact of the adhesive stresses on the shape of the surfaces [54–56].

**Impact of the decay length.** In the course of the transition between DMT to JKR, the contact equations are primarily affected by the decay length of the interactions as defined by equation (15) and encapsulated in the Tabor parameter  $\lambda$ . The finer details of the interaction potential do not affect the contact equations to first order [17]. This consideration explains: (1) why the weak formulation of the self-consistency equation is effective; (2) why a model such as Schwarz's mixed model can easily be matched to very different solutions such as Maugis' [19], as demonstrated by Carpick [57]. In fact, the details of the interaction between surfaces is often only moderately well known. Then we do not need to bother about a model which consistently takes these details into account. The most adequate model will be the simplest; in this respect Schwarz's mixed model [48, 57] and Greenwood's double-Hertz [49] are good candidates. Note, however, that the type of interactions assumed in [48] is somewhat

physically unorthodox. Worse still one cannot (explicitly or even implicitly) define an exact *interaction potential* from which the 'double-Hertz' model could possibly derive [49]. This impossibility results from the approximation involved in the weak formulation of the self-consistency.

#### 2.4. When there is more than one decay length

In some rare cases, however, we *do* know enough about the interaction potential for more elaborate models to be valuable, as when the combined measurement of both the contact *and* the non-contact parts of the force–distance curve (in the surface forces manner of section 1.2.2) is carried out. Information derived from the non-contact part of the curve can then be fed into the contact model. Experimentally, however, the consistent measurement of both contact and non-contact parts is demanding as it requires a very stiff *and* very sensitive measuring system.

A good example of such combined measurements were obtained on a stiff SFA developed in LTDS (Lyon, France) [58]. In this original device, the force and the penetration are measured but not the contact radius. The contact and interactions between silica surfaces (radius 2 mm) in a dry environment has been measured [59]. The plot (figure 11) should be compared with figure 6 a for its contact part ( $\delta > -1$ ). The non-contact part ( $\delta < -1$ ) reveals a linear interaction potential, i.e. a constant Laplace pressure resulting from a liquid meniscus. The slope directly provides a measurement of the interaction stress  $\sigma_0 \simeq 6$  MPa resulting in  $\lambda \simeq 0.3$ . However, a striking feature is the force jump between the contact and the non-contact parts of the curve. Indeed a simple meniscus model such as developed by Maugis [19, 60] implies continuity between the two parts of the curves for  $\lambda = 0.3$  and rules out such a jump.

This experimental result reveals that another attractive interaction is present in addition to the meniscus force. This additional interaction has a very short range. A model has been developed to take both contributions into account [61]: the long range interaction (the meniscus force, described as in the Maugis model by a constant stress zone with  $\lambda \simeq 0.3$ ) accounts for two-third and the short range interaction (similarly

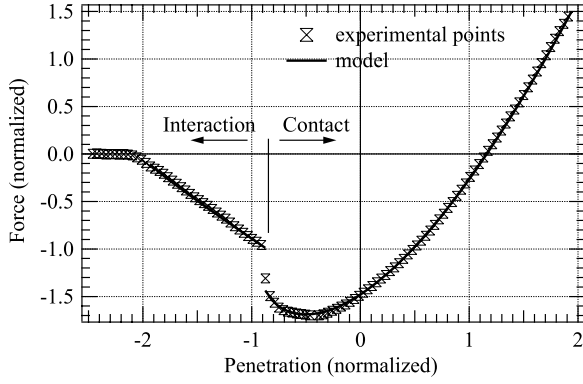


**Figure 11.** Contact and long range interactions between silica surfaces in dry air. The model fits both parts of the curve: contact and interaction simultaneously. For that purpose it must include two interaction potentials with very different decay length. (After [61] with permission from Taylor and Francis.)

described, but with a very large  $\lambda$  arbitrarily taken as 10) for one-third of the total adhesion. Thus the simultaneous fit of both contact and non-contact parts of the curve [27], involving two very different kinds of interactions, allows a clear breakdown of the total adhesion energy into each contribution.

In fact similar situations are not unfrequent. In particular, in many cases a long range repulsion is added to a short range attraction. This is the case for charged surfaces in a polar liquid. Both contributions can be taken into account in a convincing assessment of the adhesion force [62]. Similar attempts to evaluate the relation between long range interactions and adhesion energy have been carried out by ultra-high vacuum AFM forces measurements [63, 64].

In summary, finite range interactions

- (i) introduce a flat punch term as in the JKR model, but with reduced amplitude,
- (ii) introduce an outer force term as in the DMT model, but with reduced amplitude,
- (iii) regularize the JKR singularity at the contact edge.

If the interaction features a single decay length, the relative weight of the JKR and DMT contributions is set by the Tabor parameter  $\lambda$  and a transition from DMT to JKR is followed as  $\lambda$  increases from zero to infinity. In the description of this transition, many models have been proposed which appear quite equivalent. It is only with a detailed knowledge of the interaction that specific models need to be considered.

### 3. Level 3—adhesive contact—size effects, time effects

The previous developments are relevant for homogeneous time-independent systems. We now want to push the theory further and take into account more advanced surface responses: non-homogeneous or time dependent systems. Such extensions are relatively simple in the DMT limit because the attractive interaction stresses do not bring about surface deformation so that the adhesive case is directly derived from the adhesionless solution. In other cases, the mechanical

responses of the cohesive zone and the contact zone may differ because of the different lengthscales or timescales involved. We must now consider the relation between local adhesive phenomena and macroscopic contact variables in this more general context.

#### 3.1. Adhesive contact—non-homogeneous/non-linear

**3.1.1. Non-homogeneous materials—thin films.** As soon as the JKR test was applied to the investigation of polymer interfaces the limitations due to finite sample sizes became apparent. Indeed approximately spherical lenses are more easily fabricated if thin. More importantly surface modification by coating deposition is a major field in polymer science and technology. Investigations with thin lenses [39, 65, 66] and characterization of thin films [39, 67, 68] necessarily question the assumption of *homogeneous* material response. Indeed in figure 8, the system presented a thin organic film at the surface, the impact of which has not been explicitly assessed. With such finite size issues in mind, a closer investigation of the relation between flat punch displacement and cohesive zone parameters must be carried out. We first examine the impact of an elastic coating on the relation between adhesion and flat punch displacement. Here we follow Shull [68] and resort to the compliance method.

**3.1.2. Compliance method.** In complete analogy to fracture mechanics methods, we first proceed [28, 68] to calculate the total elastic energy  $\mathcal{E}$  for a given loading. In the spirit of the JKR model, we split the total surface stress and surface displacement fields into their non-adhesive ( $\sigma_H$  and  $u_H(r)$ ) and adhesive (flat punch) components ( $\sigma_{fp}$  and  $u_{fp}(r)$ ). Since  $u_{fp}(r) = \delta_{fp}$  is uniform over the contact zone and surface stresses are zero outside the contact zone, the total elastic energy [69] is

$$\mathcal{E}(a, \delta_{fp}) = \mathcal{E}_H(a) + \frac{1}{2} S(a) \delta_{fp}^2 + F_H(a) \delta_{fp}, \quad (49)$$

where  $\delta_{fp}$  is negative.

The energy release rate  $G$  as defined in section 1.3.3 is the differential of the total energy  $\mathcal{E}(a, \delta_{fp})$  with respect to contact area  $A = \pi a^2$  at constant *total* penetration  $\delta = \delta_H(a) + \delta_{fp}$ . We have

$$\left. \frac{d\mathcal{E}}{da} \right|_{\delta} = \frac{\partial \mathcal{E}}{\partial a} + \frac{\partial \mathcal{E}}{\partial \delta_{fp}} \frac{d\delta_{fp}}{da} \quad (50)$$

and

$$d\mathcal{E}_H = F_H(a) d\delta_H, \quad (51)$$

$$dF_H = S(a) d\delta_H. \quad (52)$$

Equation (52) holds because the stress distribution goes to zero at the edge of the contact (adhesionless contact) [69].

We obtain

$$2\pi a G = \frac{1}{2} \delta_{fp}^2 \frac{dS}{da}, \quad (53)$$

a result independent of the punch shape. With  $G = w$ , equation (53) is the proper generalization of equation (28) which is recovered by inserting the contact stiffness of a homogeneous system (equation (34)).

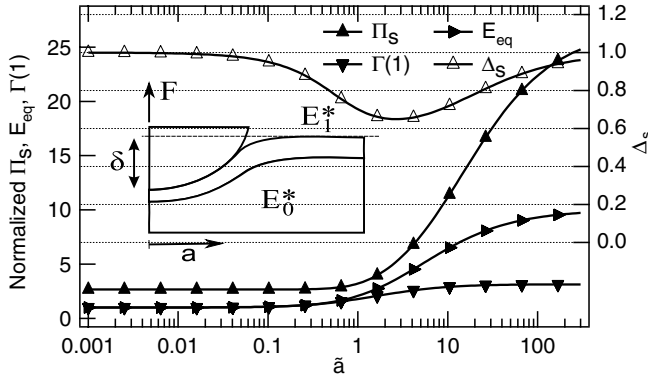


**Figure 12.** Macroscopic contact variables for a compliant film on a more rigid substrate as a function of contact radius, normalized to the film thickness  $t$ . The compliance ratio is 10.  $\Pi_s$  and  $\Delta_s$  are the normalized force and penetration for a sphere,  $E_{eq}$  is the equivalent modulus (or normalized contact stiffness) and  $\Gamma(1)$  is the correction to the stress intensity factor (equation (61)). (After [69] with permission from IOP Publishing.)

**3.1.3. Thin film—contact equations.** For a coated substrate (figure 12, inset), the contact equations for the adhesive contact of a punch of arbitrary shape is

$$\delta(a, t, [E]) = \delta_H(a, t, [E]) + \delta_{fp}, \quad (54)$$

$$F(a, t, [E]) = F_H(a, t, [E]) + S(a, t, [E])\delta_{fp}, \quad (55)$$

where the adhesionless contact variables  $\delta_H$ ,  $F_H$  and  $S$  now also depend upon the film thickness  $t$  and the various elastic parameters  $[E]$  (moduli and Poisson ratios of the film and the substrate). The flat punch displacement  $\delta_{fp}$  is determined by equation (53).

The functions  $F_H(a, t, [E])$ ,  $\delta_H(a, t, [E])$  and  $S(a, t, [E])$  may be calculated by the finite element method (FEM) [66, 68, 70–72]. Direct quasi-analytical methods have also been proposed [73–76]. They are based on the analytical calculation of the Green's function through Hankel transform. The numerics is then limited to a combination of a Fourier transform and the solution of a linear system of equations [75]: a considerably lighter task than FEM. Moreover, the generalization to a multilayer can be carried out [77].

A representative behaviour for these quantities are plotted in figure 12 for a film ten times more compliant than the substrate. When the contact radius  $a$  is much smaller than the film thickness  $t$  the system is dominated by the film elasticity  $E_1^*$ . When  $a \gg t$ , the force  $\Pi_s$  and the compliance  $E_{eq}$  are dominated by the substrate response  $E_0^*$ . A transition between these two regimes is evidenced for  $a \simeq t$ . Interestingly, the penetration  $\Delta_s$  also deviates from the simple Hertzian result  $a^2/R$  during the transition. As alluded to earlier this result attests to the mechanical origin of equation (2).

**Pull-out force.** We may expect the transition from film-dominated to substrate-dominated regimes around  $a \simeq t$  to affect the pull-out force strongly. In fact this is not the case and we now explore why. Let us first assess the impact of the film on the adhesive response when the characteristic adhesive contact radius (equation (10)) is large compared with

the film thickness [70, 78]. The elastic response relevant to the adhesionless force term  $F_H$  and to the contact stiffness  $S$  is the substrate modulus  $E_0^*$ . From equations (53) and (55), minimizing as in section 1.2.4, we obtain the typical JKR pull-out force equation (37). As a result identical pull-out forces are expected in the two limit cases (very small or very large contact radii). More generally the same characteristic size is involved in the Hertz term and the flat punch term so that the stiffnesses involved observe a parallel evolution. As a result the pull-out force is overall little affected by the presence of a film, even in the transition regime where the adhesive contact radius is close to the film thickness [69, 71, 72]. A typical deviation is in the 10–30% range.

In the absence of sizeable impact on the contact equations, we now examine the local stress field at the contact edge. In this respect, coated systems are quite different from homogeneous half spaces. To illustrate this concept we now introduce the relevant mechanical parameter, the *stress intensity factor*, which characterizes the elastic field close to the contact edge.

### 3.2. The stress intensity factor

In the context of the adhesive contact we define the *stress intensity factor*<sup>5</sup> as the quantity

$$g(a) = \int_a^{+\infty} \frac{s\sigma_z(s)}{\sqrt{s^2 - a^2}} ds. \quad (57)$$

Note that  $g(a)$  depends only upon the attractive interaction stresses which operate inside the cohesive zone.

**3.2.1. The JKR model and the stress intensity factor.** As shown in the appendix (equation (A.13)), for *homogeneous, time-independent systems*,

$$w = \frac{2g(a)^2}{\pi E^* a}. \quad (58)$$

The stress intensity factor is also directly related to the flat punch displacement by (equation (A.34)):

$$g(a) = \frac{E^*}{2} \delta_{fp}. \quad (59)$$

These two relations exemplify the role of the stress intensity factor  $g(a)$  which provides the connexion between the macroscopic contact variables (equation (59)) and the local physical process of adhesion (equation (58)). As with the flat punch displacement,  $g(a)$  characterizes the amplitude of the singularity at the contact edge (section 1.2.4).

In the JKR model, the pivotal relation (equation (28)) actually lumps together these two relations which must be analysed separately in cases more elaborate than homogeneous time-independent system.

<sup>5</sup> In terms of linear elastic fracture mechanics,  $g(a)$  has the meaning of a mode I stress intensity factor  $K$  for an outer circular crack [79] when the adhesive contact is viewed as a crack opening or closing around the contact zone [36]. The exact relation between  $g(a)$  and  $K$  is actually

$$K = \frac{2g(a)}{\sqrt{\pi a}}. \quad (56)$$



**3.2.2. Local response—thin films.** Usually, it can be assumed that the cohesive zone is small compared with the film thickness  $t$  [69, 70]. Then the local relation (equation (58)) is preserved. However, it is the film modulus  $E_1^*$  which is involved:

$$G = w = \frac{2g(a)^2}{\pi E_1^* a}. \quad (60)$$

The more general case where cohesive zone size and film thickness are comparable has also been considered [80].

For our purpose, the major impact is on the relation between stress intensity factor and flat punch penetration: if a coating is present the same stress intensity factor is obtained for a different flat punch displacement than if the material is homogeneous (equation (59)). One can define the function  $\Gamma$  such that

$$g(a) = \Gamma(a, t, [E]) \frac{E_1^*}{2} \delta_{fp}. \quad (61)$$

Following the compliance method [68], comparison between equations (53), (58) and (61) demonstrates that  $\Gamma$  can be derived from the contact stiffness as

$$\Gamma^2 = \frac{1}{2E_1^*} \frac{dS}{da}. \quad (62)$$

In fact Sridhar and Johnson [70–72] actually calculated the stress intensity factor by FEM. Interestingly the derivative method [81] they used is closely connected to the compliance method [68]. The quasi-analytical method, on the other hand, is actually based on the  $g$  function so that the stiffness and the stress intensity factor are calculated directly [69], which allows the validity of equation (62) to be checked numerically.

A representative behaviour for the function  $\Gamma$  is also displayed in figure 12 where it is indeed seen to track the contact stiffness according to equation (62). As a result of equation (62), the local field at the contact edge is significantly affected by the film. For  $a \gg t$ ,  $S = 2aE_0^*$ ,  $\Gamma = \sqrt{E_0^*/E_1^*}$  and compared with the homogeneous substrate,  $g(a)$  is multiplied by a factor  $\sqrt{E_1^*/E_0^*}$ . On the mechanical side, this alteration of the local stress field at the contact edge is the main impact of the film, which otherwise does little to affect the macroscopic response. Similar relations between remote loading and crack tip field are found in other systems [82].

**3.2.3. Material non-linearity and finite size effects.** Even homogeneous systems will exhibit finite size effects if pushed into a large deformation regime. Elastomers, which are often used with the JKR test, may undergo such large deformations.

As with thin films (section 3.1.1) the Hertz result no longer applies. A connexion can still be made with JKR theory if the adhesive solution is calculated as a *linear* perturbation to a non-linear solution. For these cases of comparatively weak adhesion, the compliance method (3.1.2) has been shown to be appropriate by Lin and coworkers [83]. Using FEM, they computed the adhesionless force, penetration and compliance in the non-linear regime. The energy release rate is calculated by equation (53) and with linear superposition the flat punch response is added to the non-linear adhesionless contact solution as in equations (31) and (32).

This paper is mainly based on linear elasticity. We also assume that the response of flat surfaces apply to moderately curved punches. The results by Lin *et al* provide insight into the limitations incurred by these standard assumptions. For instance the large deformation calculations evidence that the two following configurations are quite different:

- (i) rigid sphere on hyper-elastic flat,
- (ii) hyper-elastic sphere on rigid flat.

Let us normalize the contact stiffness by the linear result (equation (34)). In these specific calculations [83], the normalized contact stiffness of a hyper-elastic sphere pressed against a rigid surface *increases by about a factor of two* when  $a \simeq R/2$  while it *decreases by a small amount* when a rigid sphere is pressed against a hyper-elastic half-space. This contrasted behaviour results from the more constricted volume available for deformation in the case of the (hyper)-elastic sphere. The standard (linear) theory does not differentiate these two cases.

Remarkably the *force* dependence upon contact radius is moderately perturbed when going over to the non-linear regime [83, 84], in contrast to the penetration. Similar considerations apply to finite size effects in the linear regime (section 3.1.3) as can be checked in figure 12 where the *force* is seen to deviate from the film limit at larger contact radii than the penetration. The rationale is that the force is an integral quantity (equation (A.8)) and the correction comes out as a second order term. The penetration, which directly results from the stress boundary conditions (equation (A.6)), is affected by a first order correction. More detailed studies would improve our understanding of these questions but the results strongly suggest that in practice, the force versus contact radius plot is less sensitive to non-linear effects than the penetration plot. Fortunately this is the most frequent experimental set-up.

### 3.3. Adhesive viscoelastic contact—time dependent response

Time dependence is another type of interesting material response. It is mainly relevant for polymers close to their glass transition temperatures. Silicate glasses are also concerned. For example moulding viscoelastic materials is a process which can benefit from a better understanding of the viscoelastic adhesive contact [85, 86].

Referring to the mixed boundary conditions (section 1.1.1 and figure 4), we can observe that a time dependent response will affect both the cohesive zone and the contact zone but through different processes: creep is involved in the cohesive zone (under stress boundary conditions) while stress relaxation is relevant in the contact zone (under displacement boundary conditions).

We use the simplest time dependent linear response. Assuming a constant Poisson ratio, the stress  $\sigma$  and deformation  $\epsilon$  obey

$$\sigma(t) = \frac{1}{2} \int_0^t d\tau \psi(t - \tau) \frac{d}{d\tau} \epsilon(\tau), \quad (63)$$

$$\epsilon(t) = \frac{1}{2} \int_0^t d\tau \phi(t - \tau) \frac{d}{d\tau} \sigma(\tau), \quad (64)$$

where the stress relaxation function  $\psi(t) \equiv E^*_0 \tilde{\psi}(t)$  and the creep function  $\phi(t) \equiv E^*_0{}^{-1} \tilde{\phi}(t)$  are inverse for this product of convolution. The instantaneous modulus is denoted  $E^*_0$ , the long time modulus  $E^*_\infty$ . The characteristic creep time is  $T$  and the stress relaxation time is  $E^*_\infty T / E^*_0$ .

For significantly viscoelastic materials the ratio  $E^*_\infty / E^*_0$  is typically much smaller than unity; the characteristic timescales for creep and relaxation differ markedly so that it often occurs that only creep, the slowest of these two processes, is operative within the experimental timescale [87]. We consider first the issue of creep in the cohesive zone (section 3.3.1), then couple it to stress relaxation in the contact zone (section 3.3.2).

**3.3.1. Time dependent materials—creep in the cohesive zone.** This process is central to the viscoelastic crack tip theory developed by Schapery in the 1970s [25, 88–90]. It requires a cohesive zone with finite size (section 2.3) to avoid infinite strain rates [91]. Because it involves specific cohesive zone behaviour, the stress intensity factor  $g(a)$  is the adequate mechanical variable (section 3.2).

Several equivalent expressions have been developed for arbitrary [47, 92] or small [25, 88, 91] cohesive zone sizes  $\epsilon \equiv c - a$ . In the latter case, for  $\epsilon \ll a$ , the stress intensity factor  $g(a)$  may be approximated [93] by

$$g(a) \simeq -\frac{\pi}{4} \sigma_0 \sqrt{2a\epsilon}. \quad (65)$$

For an elastic cohesive zone (equation (58)), the zone size<sup>6</sup> is

$$\epsilon_0 = \frac{4}{\pi} \frac{w E^*_0}{\sigma_0^2}. \quad (66)$$

The stress intensity factor at the crack tip, for a receding contact radius (similar to an opening crack), is determined by [93]

$$w = \frac{2g(a)^2}{\pi a E^*_0} \tilde{\phi}_{\text{op}}(t_r), \quad (67)$$

which is the direct extension of equation (58). The characteristic time for the cohesive zone (figure 13) is the dwell time

$$t_r = \frac{\epsilon}{\dot{a}}, \quad (68)$$

i.e. the time for the cohesive zone to move across its width  $\epsilon$ . The effective compliance is

$$\tilde{\phi}_{\text{op}}(t) = \frac{2}{t^2} \int_0^t \tau \tilde{\phi}(\tau) d\tau. \quad (69)$$

If  $\tilde{\phi}$  is exponential with characteristic time  $T$ ,  $\tilde{\phi}_{\text{op}}(t)$  has an exponential-like behaviour with a characteristic time  $\tilde{T} \simeq 3/2 T$ .

The cohesive zone involves the material response at a characteristic time  $t_r$ . Two limit cases appear: at very low velocities the solution is elastic with the relaxed modulus. At very high velocities the crack tip is also elastic with the

<sup>6</sup> For an interesting discussion of the size of the cohesive zone for soft materials, see [94].

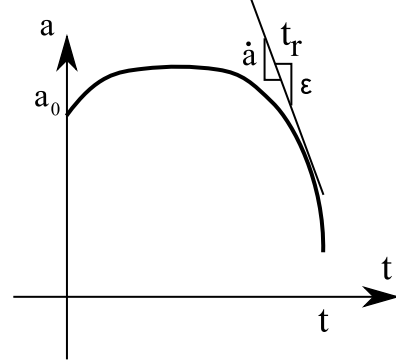


**Figure 13.** Viscoelastic contact: contact radius history and definition of the cohesive zone parameters.

instantaneous modulus: the stress intensity factor is larger by a factor  $\sqrt{E^*_0 / E^*_\infty}$ . In the intermediate regime, the strain rate depends upon the contact edge velocity  $\dot{a}$  and the cohesive stress  $\sigma_0$ . The transition occurs around

$$\dot{a}_0 \simeq \frac{\epsilon_0}{T} \quad (70)$$

so that the  $\dot{a}$  dependence of  $g(a)$  is strongly affected by the cohesive stress  $\sigma_0$  since the cross-over velocity scales with  $\sigma_0^{-2}$  (equation (66)).

**3.3.2. Time dependent materials—stress relaxation in the contact zone.** The crack tip viscoelasticity has now been accounted for. Here, in addition, we consider stress relaxation within the contact zone. The *adhesionless* viscoelastic contact problem has been intensively studied in the 1960s [95–97]. The difficulty is mainly to take into account the time dependent residual deformation for a decreasing contact radius. Similar issues must be overcome when adhesion is present. The full solution is of some complexity [47] but can be considerably simplified in many practical cases [86, 93]. Here, in the spirit of the previous sections, we emphasize the features of the theory in relation to the contact equations, focussing on contact rupture. The exact expressions for contact rupture are cluttered with ancillary terms which often contribute little to the final result. Here for simplicity we assume that the loading to the initial contact radius  $a_0$  is instantaneous. Also we consider the final phase of pull out where the contact radius at  $t$ ,  $a(t)$ , is smaller than  $a_0$  (figure 13). We denote  $\tilde{F}_H$  the geometrical factor in the Hertzian force, i.e.  $F_H = E^* \tilde{F}_H$  (appendix A.1.3). Then the contact equations are

$$g(a(t), t) = \frac{E^*_0}{2} \int_0^t d\tau \tilde{\psi}(t - \tau) \frac{\partial}{\partial \tau} (\delta(\tau) - \delta_H(r)), \quad (71)$$

$$F(t) = E^*_0 \tilde{\psi}(t) \tilde{F}_H(a(t)) + 4a(t)g(a(t), t). \quad (72)$$

Put  $g(a) = 0$  and you recover the adhesionless results [97]. Equation (71) is the generalization of equation (31) (with equation (59)). The force equation (72) generalizes equation (32) (with equation (59)). Most evident is the relaxation of the contact stresses embodied by the first term, the Hertz-like term with timescale  $t$ . The second term  $4ag(a)$  is exactly the flat punch term  $S(a)\delta_{\text{fp}}$  (equations (34) and

(59)). The characteristic timescale for this second term is therefore quite different: it is the cohesive zone dwell time  $t_r$  (equation (67)).

**Fast relaxation.** Macroscopic equations such as equations (71) and (72) can be coupled with the  $\dot{a}$ -dependence of  $g(a)$  (section 3.3.1) into a time differential equation for the contact radius  $a$ . Integration provides a solution to the full adhesive contact of viscoelastic solids [93].

More qualitatively, following Johnson [87] we can consider the case where the experimental timescale  $t$  is long compared with the relaxation time  $E_\infty^* T / E_0^*$ . This is precisely the case of elastomers, for instance (section 1.3.2).

During contact rupture, under the same conditions as equations (71) and (72)

$$g(a(t)) \simeq \frac{E_\infty^*}{2} (\delta(t) - \delta_H(a(t))), \quad (73)$$

$$F(t) \simeq E_\infty^* \tilde{F}_H(a(t)) + 4ag(a(t)). \quad (74)$$

Here the penetration depends upon the relaxed modulus, as does the Hertzian term in the force. However, the flat punch force term remains controlled by the cohesive zone response with characteristic timescale  $t_r$ .

If the contact edge moves slowly, the characteristic response is the relaxed modulus,  $\tilde{\phi}_0(t_r) = E_0^* / E_\infty^*$ ,  $2g(a)^2 = \pi a w E_\infty^*$  and the elastic case reappears, with the relaxed modulus.

If the contact edge is fast, as expected during pull out, the contact edge elasticity is set by  $E_0^*$ ,  $\tilde{\phi}_0(t_r) = 1$  and  $2g(a)^2 = \pi a w E_0^*$ . Inserting into equations (73)–(74), we can compare the dynamic contact rupture to the static contact (infinitely slow). Then for a fast crack, the apparent energy release rate for contact rupture is enhanced

$$G_{\text{app,op}} = \frac{E_0^*}{E_\infty^*} w \quad (75)$$

and the stress intensity factor  $g(a)$  is multiplied by  $\sqrt{E_0^* / E_\infty^*}$  as noted above.

During pull out, the relevant compliances for the contact and the flat punch terms are different. In this limit case, the relaxed modulus is relevant at the macroscopic scale, for the contact zone. However, it is the instantaneous modulus which is relevant for the cohesive zone resulting in an enhancement of the pull-out force by a factor of  $E_0^* / E_\infty^*$ .

**Application to cyclic loading of dissipative contacts.** A direct application of the viscoelastic response of the contact edge has been suggested by Wahl and coworkers [98]: in dynamic adhesive contact experiments performed with a nanoindenter, where the punch is oscillated at various frequencies, they have evidenced a transition from JKR contact response at low frequency to flat punch response at high frequency (figure 14). The transition can be explained [99] as follows. At low frequency the effective elastic modulus of the cohesive zone is the long time modulus  $E_\infty^*$  and the dynamic stress intensity factor  $g(a)$  is small (equation (67)). For a large enough dynamic flat punch displacement  $\delta_{fp}$  (equation (59) in which  $E^*$  is typically the long time modulus  $E_\infty^*$ ), the conditions are met

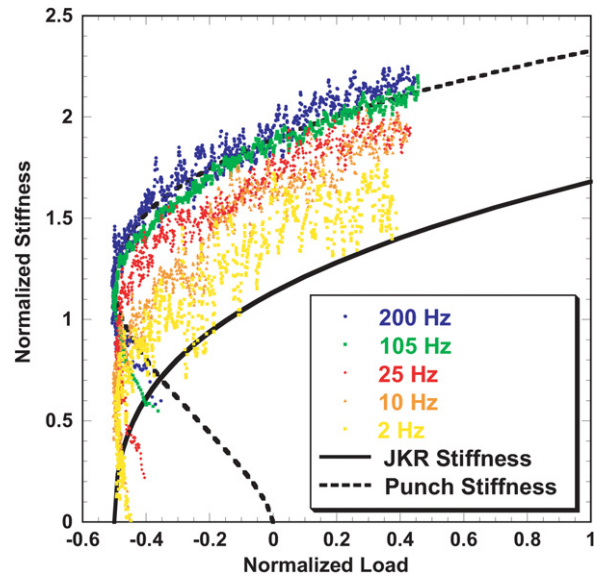


**Figure 14.** Normalized contact stiffness versus load for a sphere contacting a PDMS flat. The stiffness is measured from the AC response at varying frequencies. A transition from JKR stiffness to flat punch stiffness is evidenced as the frequency increases. (After [98] with permission from Elsevier.)

(This figure is in colour only in the electronic version)

for peeling and contact edge motion. Then the linear response is the differential  $dF/d\delta$ , the JKR contact stiffness. At larger frequencies the effective cohesive zone elastic modulus is larger (equation (67)): for an identical dynamic  $\delta_{fp}$ ,  $g(a)$  is too large for the contact radius to move and the contact edge is effectively pinned. Then the linear response is  $dF/d\delta|_a$ , which is the flat punch stiffness.

In summary, for *non-homogeneous systems* such as coated substrates, limited impact on the pull-out force is incurred because the Hertzian and flat punch force terms eventually depend upon similar elastic responses. For *time dependent systems*, in contrast, the relevant timescales during contact rupture are the contact duration for the Hertzian term and the cohesive zone dwell time for the flat punch term. This disparity typically results in a strong contrast in the relevant characteristic elastic responses and significant pull-out force enhancement. In both cases the mechanical response relevant for the cohesive zone differs from the macroscopic contact response.

## 4. Conclusion

The original contact model by Hertz has been developed for adhesionless, elastic and homogeneous half spaces. It has gradually been augmented to account for adhesive interactions and more complex mechanical responses. In this review, we have surveyed the different methods developed for that purpose. We have focused the discussion on the structure of the contact equations because they directly reveal the underlying mechanism for adhesion and their limitations.

The initial attempt by Derjaguin in 1934 to incorporate adhesion energy in the Hertz model is inaccurate but provides a qualitative answer through an elementary derivation. In

the DMT model, for weak adhesive interaction stresses, the cohesive zone extends widely around the contact zone and the energy is transferred through the work of the interaction stresses in the ('rigid body') *displacement of the punch*; actually not exactly that of a rigid body because elastic deformation occurs but it is solely due to contact stresses and it is only marginally coupled to the adhesive process. The resulting outer force term, which is added to the Hertzian contact term, depends primarily upon the interplay between interaction decay length and undeformed punch shape. In the special case of the sphere, it can usually be approximated by a constant  $-2\pi V_0 R$ . In the JKR model, for strong adhesive interaction stresses, adhesion energy is transferred during the *motion of the contact edge* as in a fracture tip. This situation is reflected in the presence of a neck at the contact edge. In the model the neck translates into a flat punch displacement. The flat punch displacement induces the required peeling action at the edge of the contact. It adds corrective terms both to the penetration and the force equations.

For intermediate values of the interaction stresses the contact equations feature both the outer force term and the flat punch contribution resulting in the well known transition from DMT to JKR. The transition parameter is the ratio of the adhesive interaction stresses to the contact stresses (the Tabor parameter) and the transition is spanned when the parameter goes from 0 to infinity. In the intermediate regime a self-consistent calculation is called for. However, the transition is very moderately dependent upon the details of the interactions and simple approximations have been developed to avoid extensive calculations. Only when a detailed description of the interaction stresses exist are more elaborate models useful.

The most recent results have focused on non-homogeneous or time dependent systems. In these more complex systems the cohesive zone and contact zone experience different mechanical responses due to the different length- or timescales. The impact of this disparity on the contact equations can be assessed, comparing the characteristic responses of the Hertzian term and the flat punch term. For a coated substrate the relevant elastic responses are similar so that little impact is registered on the pull-out force. This result applies even to the transition region where the typical adhesive contact radius is of the order of the film thickness. By contrast for time dependent systems, the elasticity of the Hertzian term is ruled by the *contact time* while the flat punch displacement is controlled by the *cohesive zone dwell time*. The latter is typically much shorter, leading to a strong enhancement of the pull-out force.

Important issues have been left out of this review. The impact of roughness [100, 101], which is of paramount experimental significance, has not been considered here, even though interesting issues arise: because the contact problem is non-linear, roughness offsets the balance between compressive and tensile stresses and strongly affects adhesion. Plastic deformation, with more limited literature available, also certainly needs consideration in practice [102–104]. Here the strategy is similar to the non-linear adhesive contact (section 3.2.3). Finally the wide area of elastic contacts under *tangential* loading and friction, with numerous practical issues,

is also amenable to the Hankel transform technique and could be considered as a different but adjacent perspective.

## Acknowledgments

The author thanks the many colleagues with whom he interacted either directly or by mail and to whom he is indebted for many of the ideas developed in this paper, and especially D Maugis and K Johnson.

## Appendix A. Level 4—calculation methods

### Appendix A.1. The stress method

*Appendix A.1.1. Abel transforms and equilibrium.* Adequate transforms facilitate the investigation of linear elastic axisymmetric contacts formulated as integral equations [10, 105]. Following Sneddon [10, 17, 47, 61, 93], we use  $g(r)$ , which is an Abel transform of the normal stress distribution at the surface  $\sigma_z$ . It is defined by

$$g(r) = \int_r^{+\infty} \frac{s\sigma_z(s)}{\sqrt{s^2 - r^2}} ds. \quad (\text{A.1})$$

Similarly  $\theta(r)$  is a transform of the normal surface displacement  $u_z$  [93, 106]. It is defined by

$$\theta(r) = \frac{\partial}{\partial r} \int_0^r \frac{s u_z(s)}{\sqrt{r^2 - s^2}} ds. \quad (\text{A.2})$$

These relations are suited to the adhesive contact problem because  $g(r)$  is expressed as a function of normal surface stresses at radii values larger than  $r$  and  $\theta(r)$  as a function of surface normal displacement at radii values smaller than  $r$ , in agreement with the adhesive contact boundary conditions (figure 4). For instance, for an adhesionless contact,  $g$  is zero outside the contact zone ( $r \geq a$ ). Similarly, inside the contact zone ( $r \leq a$ ),  $u_z(r) = \delta - f(r)$  where  $f(r)$  is the shape of the indenter. Integration by parts transforms equation (A.2) into

$$\theta(r) = \delta - \delta_0(r), \quad (\text{A.3})$$

where  $\delta$  is the penetration and  $\delta_0$  depends only upon the shape of the indenter  $f(r)$  through

$$\delta_0(r) = r \int_0^r \frac{f'(s) ds}{\sqrt{r^2 - s^2}}. \quad (\text{A.4})$$

*Appendix A.1.2. Equilibrium—application to the adhesive contact.* The full power of these transforms appears when it is recognized [47, 93] that in the linear elastic case and for a *homogeneous* substrate, mechanical equilibrium results in

$$g(r) = \frac{E^*}{2} \theta(r). \quad (\text{A.5})$$

Assuming continuity of the stress distribution at  $a$  (a condition similar but stronger than the postulated cancellation of inner and outer stress intensity factors in [19])

$$g(a) = \frac{E^*}{2} \theta(a). \quad (\text{A.6})$$



For an adhesionless contact  $g(a) = 0$ . Then the penetration  $\delta$  is equal to the function  $\delta_0(a)$ .

For an adhesive contact  $g(a) \neq 0$  and

$$\delta = \delta_H(a) + \frac{2}{E^*} g(a), \quad (\text{A.7})$$

which is equation (59).

*Appendix A.1.3. Integral quantities—force and energy.* The force can be obtained through [61]

$$F = 4 \int_0^{+\infty} g(s) ds. \quad (\text{A.8})$$

For an adhesionless contact the force  $F$  is equal to

$$F_H(a) = E^* \tilde{F}_H(a), \quad (\text{A.9})$$

where (equations (A.3) and (A.5))

$$\tilde{F}_H(a) = 2 \int_0^a (\delta_H(a) - \delta_0(s)) ds. \quad (\text{A.10})$$

For an adhesive contact  $g(a) \neq 0$  and

$$F = F_H(a) + 4ag(a) + 4 \int_a^{+\infty} g(s) ds. \quad (\text{A.11})$$

Inserting equation (A.1) and changing the order of integration shows that the last term is indeed equal to  $F_{\text{ext}}$  (equation (21)) resulting in equation (40).

In addition the total mechanical energy  $\mathcal{E}$  as a function of the normal surface stress distribution is [61]

$$\mathcal{E} = \frac{4}{E^*} \int_0^{+\infty} ds g^2(s) = E^* \int_0^{+\infty} ds \theta^2(s). \quad (\text{A.12})$$

Then if  $\delta$  is constant and  $g(r) = 0$  for  $r > a$ ,

$$\frac{1}{2\pi a} \frac{\partial \mathcal{E}}{\partial a} \Big|_{\delta} = \frac{2g^2(a)}{\pi E^* a}, \quad (\text{A.13})$$

which is equation (58).

*Appendix A.1.4. Inverses—gap and contact stress distribution.* The inverse relations to equations (A.1) and (A.2) are

$$s\sigma_z(s) = \frac{2}{\pi} \frac{d}{ds} \int_s^{+\infty} dr \frac{rg(r)}{(r^2 - s^2)^{1/2}} \quad (\text{A.14})$$

or

$$\sigma_z(s) = -\frac{2}{\pi} \left[ \int_s^{+\infty} dr \frac{g'(r)}{(r^2 - s^2)^{1/2}} \right] \quad (\text{A.15})$$

and

$$u_z(r) = \frac{2}{\pi} \int_0^r \frac{\theta(s)}{(r^2 - s^2)^{1/2}} ds. \quad (\text{A.16})$$

One can derive a useful expression for the gap [47]:

$$h(r) \equiv u(r) - \delta + f(r) \quad (\text{A.17})$$

$$= \frac{2}{\pi} \left\{ \int_a^r ds \frac{\delta_0(s) - \delta_0(a)}{\sqrt{r^2 - s^2}} + \int_a^r ds \frac{\theta(s) - \theta(a)}{\sqrt{r^2 - s^2}} \right\}. \quad (\text{A.18})$$

Let us investigate the behaviour of the gap  $h(r)$  for  $r \rightarrow a(t)$ . For  $r = a(1 + \epsilon)$ , one can show that, for a differentiable function  $j(s)$ ,

$$\int_a^r ds \frac{j(s)}{\sqrt{r^2 - s^2}} = (2\epsilon)^{1/2} j(a) + O(\epsilon^{3/2}). \quad (\text{A.19})$$

Thus, continuity of  $\theta$  at  $a$  entails that the second term in equation (A.19) behave as  $\epsilon^{3/2}$  at  $a$ . The Hertz term  $h_{\text{Hertz}}(r, a)$  behave similarly, since it has the same form (equation (A.26)), and therefore the  $O(\epsilon^{3/2})$  behaviour applies to the total gap (figure 9).

## Appendix A.2. Applications

*Appendix A.2.1. The sphere (a paraboloid).* For the adhesionless sphere, the boundary conditions are

$$u_{z,H}(r) = \frac{r^2}{2R} \quad \text{for } r < a, \quad (\text{A.20})$$

$$\sigma_{z,H}(r) = 0 \quad \text{for } r > a. \quad (\text{A.21})$$

From equation (A.4) one obtains

$$\delta_{0,H}(r) = \frac{r^2}{R}. \quad (\text{A.22})$$

The equilibrium equation (A.5) results in

$$\theta_H(r) = 0 \quad \text{for } r > a, \quad (\text{A.23})$$

$$g_H(r) = \frac{E^*}{2} (\delta - \delta_{0,H}(r)) \quad \text{for } r < a. \quad (\text{A.24})$$

Due to continuity of the normal stress at the edge of the contact zone,

$$\delta = \delta_{0,H}(a), \quad (\text{A.25})$$

which results in the Hertzian penetration equation (2). The force is calculated through equation (A.8) which results in equation (3). Finally the gap results from equation (A.18) using equations (A.22) and (A.23):

$$h_H(r, a) = \frac{2}{\pi} \frac{1}{R} \tilde{h}_H(r, a), \quad (\text{A.26})$$

where

$$\tilde{h}_H(r, a) \equiv \int_a^r ds \frac{(s^2 - a^2)}{\sqrt{r^2 - s^2}} = \left\{ \frac{a}{2} \sqrt{r^2 - a^2} + \left( \frac{r^2}{2} - a^2 \right) \arccos \left( \frac{a}{r} \right) \right\}. \quad (\text{A.27})$$

*Appendix A.2.2. Flat punch.* The boundary conditions are

$$u_{z,fp}(r) = \delta_{fp} \quad \text{for } r < a, \quad (\text{A.28})$$

$$\sigma_{z,fp}(r) = 0 \quad \text{for } r > a. \quad (\text{A.29})$$

From equation (A.4) one obtains

$$\delta_{0,fp}(r) = 0 \quad (\text{A.30})$$

so that

$$\theta_{fp}(r) = \delta_{fp} \quad \text{for } r < a, \quad (\text{A.31})$$

$$g_{fp}(r) = 0 \quad \text{for } r > a. \quad (\text{A.32})$$

The equilibrium equation (A.5) results in

$$\theta_{\text{fp}}(r) = 0 \quad \text{for } r > a, \quad (\text{A.33})$$

$$g_{\text{fp}}(r) = \frac{E^*}{2} \delta_{\text{fp}} \quad \text{for } r < a. \quad (\text{A.34})$$

Continuity of the normal stress at the edge of the contact zone does not apply due to the punch singularity. The contact radius is equal to the punch radius and the flat punch solution is linear in  $\delta_{\text{fp}}$ .

The force is calculated through equation (A.8) which results in

$$F_{\text{fp}}(r) = 4 \int_0^a g_{\text{fp}}(s) ds = S(a) \delta_{\text{fp}}, \quad (\text{A.35})$$

where  $S(a)$  is the contact stiffness equation (34).

The gap is not defined but the surface displacement outside the contact zone can be evaluated (equations (A.16) and (A.31)) as

$$u_{z,\text{fp}}(r) = \delta_{\text{fp}} \left( 1 - \frac{2}{\pi} \arccos \left( \frac{a}{r} \right) \right) \quad (\text{A.36})$$

with a singular behaviour at  $a$ :

$$u_{z,\text{fp}}(r) \simeq \frac{2}{\pi} \delta_{\text{fp}} \sqrt{2(r-a)}. \quad (\text{A.37})$$

Similarly, using equations (A.15), (A.32) and (A.34) we obtain

$$\sigma_z(r) = -\frac{E^* \delta_{\text{fp}}}{\pi} \frac{1}{\sqrt{a^2 - r^2}} \quad (\text{A.38})$$

with a singular behaviour at  $r = a$ :

$$\sigma_z(r) \simeq -\frac{E^* \delta_{\text{fp}}}{\pi \sqrt{2a}} \frac{1}{\sqrt{a-r}} \quad (\text{A.39})$$

### Appendix A.3. Normalization

In the case of the spheres, following [19], we normalize  $F$  by  $\pi w R$ , and introduce

$$P = \frac{F}{\pi w R}, \quad (\text{A.40})$$

$$A = \frac{a}{\left( \frac{3\pi w R^2}{4E^*} \right)^{1/3}}, \quad (\text{A.41})$$

$$\Delta = \frac{\delta}{\left( \frac{9\pi^2 w^2 R}{16E^{*2}} \right)^{1/3}}, \quad (\text{A.42})$$

$$\lambda = \frac{2\sigma_0}{\left( \frac{16E^{*2} \pi w}{9R} \right)^{1/3}}. \quad (\text{A.43})$$

## References

- [1] Eichenlaub S, Kumar G and Beaudoin S 2006 A modeling approach to describe the adhesion of rough, asymmetric particles to surfaces *J. Colloid Interface Sci.* **299** 656–64

- [2] Donnet C and Erdemir A 2004 Solid lubricant coatings: recent developments and future trends *Tribol. Lett.* **17** 389–397
- [3] Tambe N S and Bhushan B 2004 Scale dependence of micro/nano-friction and adhesion of MEMS/NEMS materials, coatings and lubricants *Nanotechnology* **15** 1561–70
- [4] Stamatakis K and Tien C 1993 A simple model of cross-flow filtration based on particle adhesion *AIChE J.* **39** 1292–302
- [5] Rimai D S, Quesnel D J, DeMejo L P and Regan M T 2001 Toner to photoconductor adhesion *J. Imag. Sci. Technol.* **45** 179–86
- [6] Horton J C, German C S, Allen S, Davies M C, Roberts C J, Tendler S J and Williams P M 2003 Characterization of particle-interactions by atomic force microscopy: effect of contact area *Pharmac. Res.* **20** 508–14
- [7] Johnson K L, Kendall K and Roberts A D 1971 Surface energy and the contact of elastic solids *Proc. R. Soc. Lond. A* **324** 301–13
- [8] Hertz H 1882 Über die berührung fester elastische körper *J. Reine Angew. Math.* **92** 156
- [9] Sneddon I N 1950 *Fourier Transform* (New York: McGraw-Hill)
- [10] Sneddon I N 1965 The relation between load and penetration in the axisymmetric boussinesq problem for a punch of arbitrary profile *Int. J. Eng. Sci.* **3** 47
- [11] Spence D A 1968 Self-similar solutions to adhesive contact problems with incremental loading *Proc. R. Soc. A* **305** 55
- [12] Derjaguin B 1934 Untersuchungen über die reibung und adhäSION, IV *Kolloid-Z.* **69** 55–164
- [13] Derjaguin B V, Muller V M and Toporov Yu P 1975 Effect of contact deformation on the adhesion *J. Colloid Interface Sci.* **53** 314
- [14] Parsegian V A 2006 *Van der Waals Forces* (Cambridge, UK: Cambridge University Press)
- [15] Bradley R S 1932 The cohesive force between solid surfaces and the surface energy of solids *Phil. Mag.* **13** 853
- [16] Hughes B D and White L R 1979 'Soft' contact problems in linear elasticity *Q. J. Mech. Appl. Math.* **32** 445–71
- [17] Barthel E 1998 On the description of the adhesive contact of spheres with arbitrary interaction potentials *J. Colloid Interface Sci.* **200** 7–18
- [18] Johnson K L and Greenwood J A 1997 An adhesion map for the contact of elastic spheres *J. Colloid Interface Sci.* **192** 326–33
- [19] Maugis D 1992 Adhesion of spheres: the JKR-DMT transition using a dugdale model *J. Colloid Interface Sci.* **150** 243–69
- [20] Triadis D 2007 Indentation models for colloid science and nanotechnology *PhD Thesis* Department of Mathematics and Statistics, University of Melbourne
- [21] Israelachvili J N 1992 *Intermolecular and Surface Forces* (San Diego, CA: Academic)
- [22] Muller V M, Derjaguin B V and Toporov Yu P 1983 On two methods of calculation of the force of sticking of an elastic sphere to a rigid plane *Colloids Surf.* **7** 251–9
- [23] Pashley M D 1984 Further consideration of the DMT model for elastic contact *Colloids Surf.* **12** 69–77
- [24] Greenwood J 2007 On the DMT theory *Tribol. Lett.* **26** 203–11
- [25] Greenwood J A and Johnson K L 1981 The mechanics of adhesion of viscoelastic solids *Phil. Mag.* **43** 697–711
- [26] Zheng Z and Yu J 2007 Using the dugdale approximation to match a specific interaction in the adhesive contact of elastic objects *J. Colloid Interface Sci.* **310** 27–34
- [27] Barthel E 1999 The adhesive contact of spheres: when the interaction is complex *Colloids Surf. A* **149** 99–105

- [28] Johnson K L 1985 *Contact Mechanics* (Cambridge, UK: Cambridge University Press)
- [29] Tabor D 1977 Surface forces and surface interactions *J. Colloids Interface Sci.* **58** 2
- [30] Greenwood J A 1997 Adhesion of elastic spheres *Proc. R. Soc. Lond. A* **453** 1277
- [31] Carpick R W, Agrait N, Ogletree D F and Salmeron M 1996 Measurement of interfacial shear (friction) with an ultrahigh vacuum atomic force microscope *J. Vac. Sci. Technol. B* **14** 1289–95
- [32] Maugis D 2000 *Contact, Adhesion and Rupture of Elastic Solids* (Berlin: Springer)
- [33] Grierson D S, Flater E E and Carpick R W 2005 Accounting for the JKR–DMT transition in adhesion and friction measurements with atomic force microscopy *J. Adhes. Sci. Technol.* **19** 291–311
- [34] Barthel E and Roux S 2000 Velocity-dependent adhesion: an analytical approach for the JKR and DMT models *Langmuir* **16** 8134–38
- [35] Chaudhury M K and Whitesides G M 1992 Correlation between surface free energy and surface constitution *Science* **255** 1230–2
- [36] Maugis D and Barquins M 1978 Fracture mechanics and the adherence of viscoelastic bodies *J. Phys. D: Appl. Phys.* **11** 1989
- [37] Vigil G, Xu Z, Steinberg S and Israelachvili J 1994 Interactions of silica surfaces *J. Colloid Interface Sci.* **165** 367–85
- [38] Deruelle M, Leger L and Tirrel M 1995 Adhesion at the solid-elastomer interface: influence of the interfacial chains *Macromolecules* **28** 7419–28
- [39] Deruelle M, Hervet H, Jandeau G and Leger L 1998 Some remarks on JKR experiments *J. Adhes. Sci. Technol.* **12** 225–47
- [40] Tay A and Barquins M 2006 Detachment of glass balls from smooth rubber under gravity *Int. J. Adhes. Adhes.* **26** 371–7
- [41] Kendall K 2001 *Molecular Adhesion and its Applications* (Dordrecht/New York: Kluwer/Plenum)
- [42] Butt H J, Capella B and Kappl M 2005 Force measurements with the atomic force microscope: technique, interpretation and applications *Surf. Sci. Rep.* **59** 1–152
- [43] Leggett G J 2003 Friction force microscopy of self-assembled monolayers: probing molecular organisation at the nanometre scale *Anal. Chim. Acta* **479** 17–38
- [44] Carpick R W, Ogletree D F and Salmeron M 1997 Lateral stiffness: a new nanomechanical measurement for the determination of shear strengths with friction force microscopy *Appl. Phys. Lett.* **70** 1548–50
- [45] Lantz M A, O'Shea S J, Welland M E and Johnson K L 1997 Atomic-force microscope study *Phys. Rev. B* 10776
- [46] Basire C and Fretigny C 1999 Determination of viscoelastic moduli at a submicrometric scale *Eur. Phys. J. Appl. Phys.* **6** 323–9
- [47] Haiat G, Phan Huy M C and Barthel E 2003 The adhesive contact of viscoelastic spheres *J. Mech. Phys. Solids* **51** 69–99
- [48] Schwarz U D 2003 A generalized analytical model for the elastic deformation of an adhesive contact between a sphere and a flat surface *J. Colloid Interface Sci.* **261** 99–106
- [49] Greenwood J A and Johnson K L 1998 An alternative to the maugis model of adhesion between elastic spheres *J. Phys. D: Appl. Phys.* **31** 3279–90
- [50] Legait B and de Gennes P G 1984 Capillary rise between closely spaced plates: effect of van der waals forces *J. Physique Lett.* **45** 647–52
- [51] Muller V M, Yushenko V S and Derjaguin B V 1980 On the influence of molecular forces on the deformation of an elastic sphere *J. Colloid Interface Sci.* **77** 91
- [52] Muller V M, Yushchenko V S and Derjaguin B V 1982 General theoretical considerations on the influence of surface forces on contact deformations *J. Colloid Interface Sci.* **92** 92
- [53] Feng J Q 2001 Adhesive contact of elastically deformable spheres: a computational study of pull-off force and contact radius *J. Colloid Interface Sci.* **238** 318–23
- [54] Horn R G, Israelachvili J N and Pribac F 1987 Measurement of the deformation and adhesion of solids in contact *J. Colloid Interface Sci.* **115** 480–92
- [55] Christenson H K 1996 Surface deformations in direct force measurements *Langmuir* **12** 1404–5
- [56] Maugis D and Gauthier-Manuel B 1994 JKR–DMT transition in the presence of a liquid meniscus *J. Adhes. Sci. Technol.* **8** 1311–22
- [57] Carpick R W, Ogletree D F and Salmeron M 1999 A general equation for fitting contact area and friction vs load measurements *J. Colloid Interface Sci.* **211** 395–400
- [58] Tonck A, Houze F, Boyer L, Loubet J-L and Georges J-M 1991 Electrical and mechanical contact between rough gold surfaces in air *J. Phys. D: Appl. Phys.* **3** 5195–201
- [59] Barthel E, Lin X Y and Loubet J L 1996 Adhesion energy measurements in the presence of adsorbed liquid using a rigid surface force apparatus *J. Colloid Interface Sci.* **177** 401–6
- [60] Kim K S, McMeeking R M and Johnson K L 1998 Adhesion, slip, cohesive zones and energy fluxes for elastic spheres in contact *J. Mech. Phys. Solids* **46** 243–66
- [61] Huguet A S and Barthel E 2000 Surface forces and the adhesive contact of axisymmetric bodies *J. Adhes.* **74** 143–75
- [62] Drummond C, In M and Richetti P 2004 Behavior of adhesive boundary lubricated surfaces under shear: effect of grafted diblock copolymers *Eur. Phys. J. E* **15** 159–65
- [63] Sounilhac S, Barthel E and Creuzet F 1999 Long range forces and adhesion energy between tungsten and TiO<sub>2</sub>(1 0 0) surfaces under ultra high vacuum *J. Appl. Phys.* **85** 222–7
- [64] Sounilhac S, Barthel E and Creuzet F 1999 The electrostatic contribution to the long-range interactions between tungsten and oxide surfaces under ultrahigh vacuum *Appl. Surf. Sci.* **140** 411
- [65] Ahn D and Shull K R 1996 JKR studies of acrylic elastomer adhesion to glassy polymer substrates *Macromolecules* **29** 4381–90
- [66] Shull K R, Ahn D and Mowery C L 1997 Finite-size corrections to the JKR technique for measuring adhesion: soft spherical caps adhering to flat, rigid surfaces *Langmuir* **13** 1799–804
- [67] Tardivat C, Hervet H and Léger L 2001 Adhesion evaluation for a stratified system in JKR geometry *J. Adhes. Sci. Technol.* **15** 1055–78
- [68] Shull K R 2002 Contact mechanics and the adhesion of soft solids *Mater. Sci. Eng. R: Rep.* **36** 1–45
- [69] Barthel E and Perriot A 2007 Adhesive contact to a coated elastic substrate *J. Phys. D: Appl. Phys.* **40** 1059–67
- [70] Sridhar I, Johnson K L and Fleck N A 1997 Adhesion mechanics of the surface force apparatus *J. Phys. D: Appl. Phys.* **30** 1710–9
- [71] Johnson K L and Sridhar I 2001 Adhesion between a spherical indenter and an elastic solid with a compliant elastic coating *J. Phys. D: Appl. Phys.* **34** 683–9
- [72] Sridhar I, Zheng Z W and Johnson K L 2004 A detailed analysis of adhesion mechanics between a compliant elastic coating and a spherical probe *J. Phys. D: Appl. Phys.* **37** 2886–95
- [73] Yu H Y, Sanday S C and Rath B B 1990 The effect of substrate on the elastic properties of films determined by the indentation test: axisymmetric boussinesq problem *J. Mech. Phys. Solids* **38** 745–64

- [74] Gao H J, Chiu C H and Lee J 1992 Elastic contact versus indentation modeling of multi-layered materials *Int. J. Solids Struct.* **29** 2471–92
- [75] Perriot A and Barthel E 2004 Elastic contact to a coated half-space: effective elastic modulus and real penetration *J. Mater. Res.* **19** 600–8
- [76] Gacoin E, Frétny C, Chateauminois A, Perriot A and Barthel E 2006 Measurement of the mechanical properties of thin films mechanically confined within contacts *Tribol. Lett.* **21** 245–52
- [77] Frétny C and Chateauminois A 2007 Solution for the elastic field in a layered medium under axisymmetric contact loading *J. Phys. D.: Appl. Phys.* **40** 5418–26
- [78] Reedy D 2006 Thin-coating contact mechanics with adhesion *J. Mater. Res.* **21** 2660–8
- [79] Lowengrub M and Sneddon I N 1965 The distribution of stress in the vicinity of an external crack in an infinite elastic solid *Int. J. Eng. Sci.* **3** 451–60
- [80] Onur-Sergici A, George G Adams and Muftu S 2006 Adhesion in the contact of a spherical indenter with a layered elastic half-space *J. Mech. Phys. Solids* **54** 1843–61
- [81] Parks D M 1974 A stiffness derivative finite element technique for the determination of crack tip stress intensity factors *Int. J. Fract.* **10** 487–502
- [82] Fleck N A, Hutchinson J W and Suo Z 1991 Crack path selection in a brittle adhesive layer *Int. J. Solids Struct.* **27** 1683–703
- [83] Lin Y Y and Chen H Y 2006 Effect of large deformation and material nonlinearity on the JKR (Johnson–Kendall–Roberts) test of soft elastic materials *J. Polym. Sci. B: Polym. Phys.* **44** 2912–22
- [84] Hui C Y, Lin Y Y and Baney J M 2000 The mechanics of tack: viscoelastic contact on a rough surface *J. Polym. Sci. B: Polym. Phys.* **38** 1485–95
- [85] Pech J, Berthome G, Jeymond M and Eustathopoulos N 2005 Influence of glass/mould interfaces on sticking *Glass Sci. Technol.* **78** 54–62
- [86] Haiat G and Barthel E 2007 An approximate model for the adhesive contact of rough viscoelastic surfaces *Langmuir* **23** 11643–50
- [87] Johnson K L 2000 Contact mechanics and adhesion of viscoelastic solids *Microstructure and Microtribology of Polymer Surfaces* ed K J Wahl and V V Tsukruk (Washington, DC: American Chemical Society) p 24
- [88] Schapery R A 1975 A theory of crack initiation and growth in viscoelastic media: II. Approximate methods of analysis *Int. J. Fract.* **3** 369–88
- [89] Schapery R A 1975 A theory of crack initiation and growth in viscoelastic media *Int. J. Fract.* **11** 549–62
- [90] Schapery R A 1989 On the mechanics of crack closing and bonding in linear viscoelastic media *Int. J. Fract.* **39** 163–89
- [91] Hui C Y, Baney J M and Kramer E J 1998 Contact mechanics and adhesion of viscoelastic spheres *Langmuir* **14** 6570–8
- [92] Greenwood J A 2004 The theory of viscoelastic crack propagation and healing *J. Phys. D: Appl. Phys.* **37** 2557–69
- [93] Barthel E and Haiat G 2002 A simple model for the adhesive contact of viscoelastic spheres *Langmuir* **18** 9362–70
- [94] Hui C-Y, Jagota A, Bennison S J and Londono J D 2003 Crack blunting and the strength of soft elastic solids *Proc. R. Soc. A* **459** 1489–516
- [95] Lee E H and Radok J R M 1960 The contact problems for viscoelastic bodies *J. Appl. Mech.* **27** 438–44
- [96] Graham G A C 1965 The contact problem in the linear theory of viscoelasticity *Int. J. Eng. Sci.* **3** 27–46
- [97] Ting T C T 1966 The contact stresses between a rigid indenter and a viscoelastic half-space *J. Appl. Mech.* **33** 845–54
- [98] Wahl K J, Asif S A S, Greenwood J A and Johnson K L 2006 Oscillating adhesive contacts between micron-scale tips and compliant polymers *J. Colloid Interface Sci.* **296** 178–88
- [99] Greenwood J A and Johnson K L 2006 Oscillatory loading of a viscoelastic adhesive contact *J. Colloid Interface Sci.* **296** 284–91
- [100] Fuller K and Tabor D 1975 The effect of surface roughness on the adhesion of elastic solids *Proc. R. Soc. A* **345** 327–42
- [101] Persson B N 2002 Adhesion between elastic bodies with randomly rough surfaces *Phys. Rev. Lett.* **89** 245502
- [102] Pollock H M 1978 Contact adhesion between solids in vacuum: II. Deformation and interfacial energy *J. Phys. D: Appl. Phys.* **11** 39–54
- [103] Mesarovic S D and Johnson K L 2000 Adhesive contact of elastic–plastic spheres *J. Mech. Phys. Solids* **48** 2009–33
- [104] Kogut L and Etsion I 2003 Adhesion in elastic–plastic spherical microcontact *J. Colloids Interface Sci.* **261** 372–8
- [105] Gladwell G M L 1980 *Contact Problems in the Classical Theory of Elasticity* (Germantown, MD: Sijthoff & Noordhoff)
- [106] Barthel E, Perriot A, Chateauminois A and Frétny C 2006 Elastic contact to nearly incompressible coatings: stiffness enhancement and elastic pile-up instrumented indentation testing in materials research and development *Phil. Mag.* **86** 5359–69